Şcoala doctorală
Anul universitar 2020/2021

Universitatea Politehnica Timişoara

Piaţa Victoriei nr. 2
RO 300006 - Timişoara
Tel: +40 256 403000
Fax: +40 256 403021
rector@upt.ro
www.upt.ro

Seminar:
Redactarea lucrărilor ştiinţifice:
Partea experimentală
Rezultate şi discuţii

Universitatea Politehnica Timişoara

Prof. dr. ing. Nicolae VASZILCSIN
Facultatea de Chimie Industrială şi Ingineria Mediului
Laborator: Electrochimie, Coroziune şi Inginerie Electrochimică

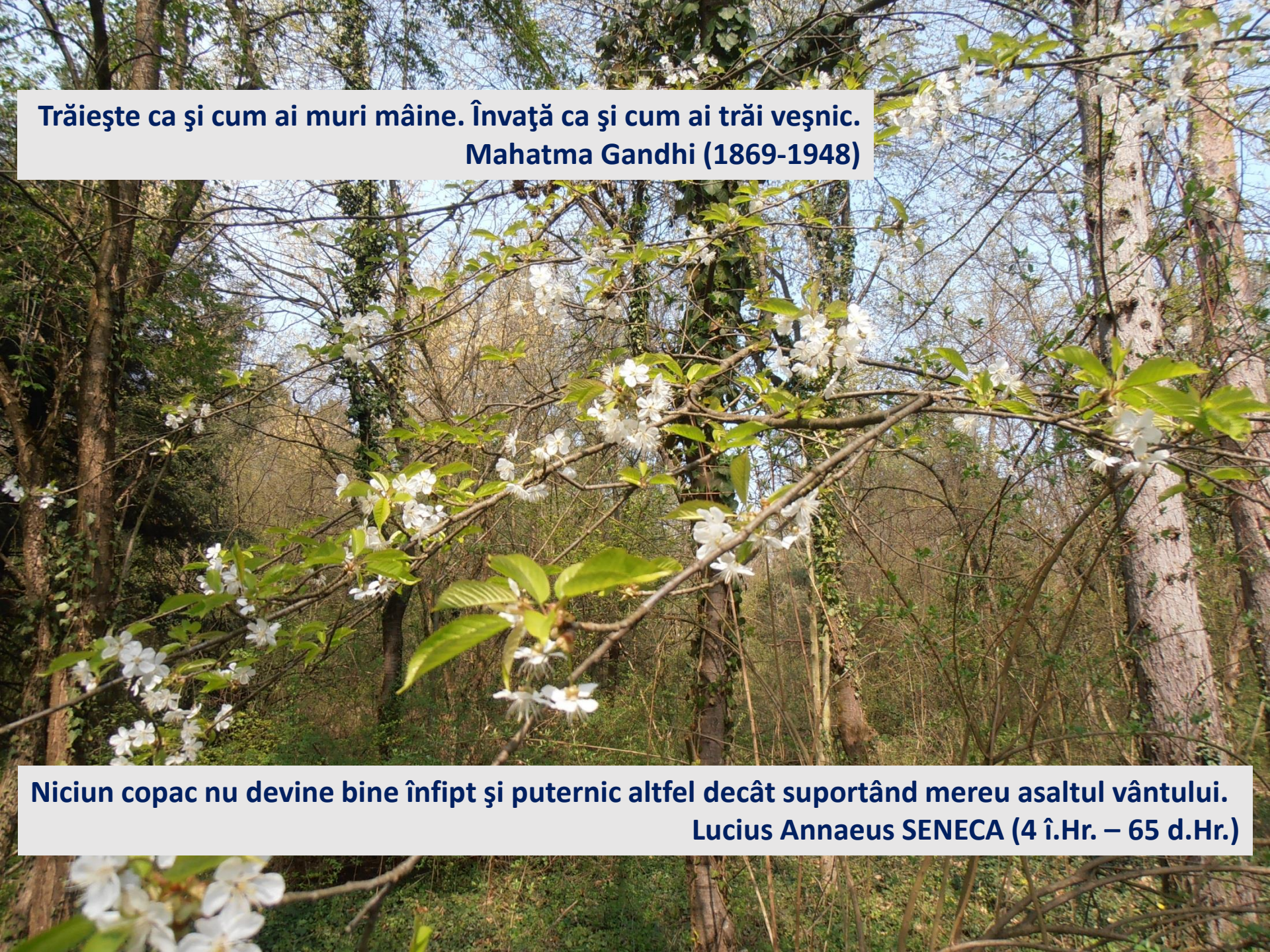

Trăieşte ca şi cum ai muri mâine. Învaţă ca şi cum ai trăi veşnic.
Mahatma Gandhi (1869-1948)

Niciun copac nu devine bine înfipt şi puternic altfel decât suportând mereu asaltul vântului.
Lucius Annaeus SENECA (4 î.Hr. – 65 d.Hr.)

Cercetarea ştiinţifică

- activitate prin care se dobândesc informaţii şi cunoştinţe despre univers

Funcţiile cercetării ştiinţifice:

- cognitivă

- formativă

- informativă

Scopul cercetării ştiinţifice: asigurarea progresului civilizaţiei

Clasificare:
Cercetare ştiinţifică fundamentală:
Cercetare ştiinţifică aplicată:

Funcţia cognitiva

- evaluare continuă, de aprofundare şi de dezvoltare a cunoaşterii, precum şi aplicaţii particulare în diferite domenii ale ştiinţei şi tehnologiei.

- Descoperirea legilor dupa care se produc fenomenele din univers. (legenda Arhimede – Evrika)

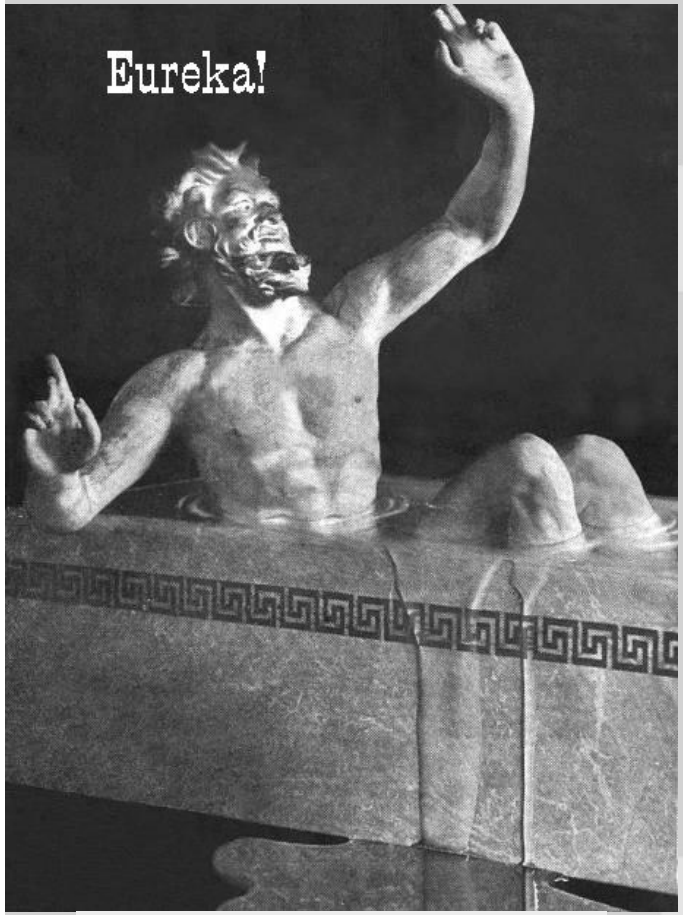

Arhimede (287 – 212 BC)

Un corp scufundat intr-un lichid este impins de jos in sus cu o forta egala cu greutatea lichidului dezlocuit.

Piaţa Victoriei nr. 2, RO 300006 - Timişoara, Tel: +40 256 403000, Fax: +40 256 403021, rector@upt.ro, www.upt.ro

Calcularea circumferintei Terrei

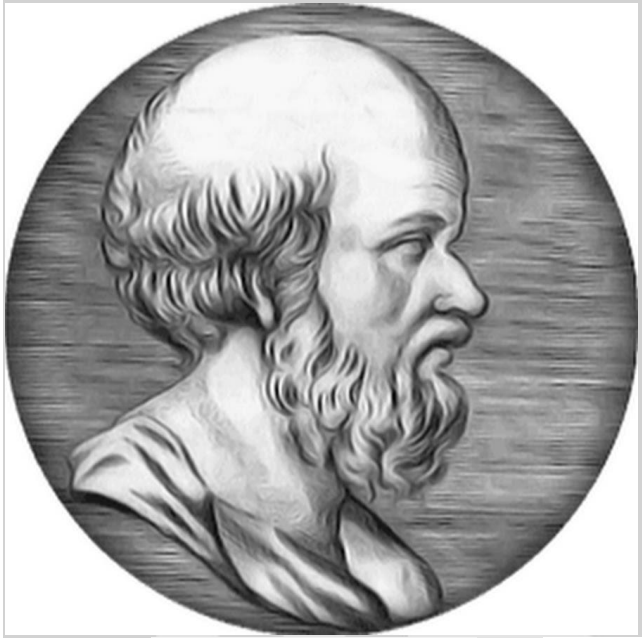

Eratostene
(276 – 194 BC)

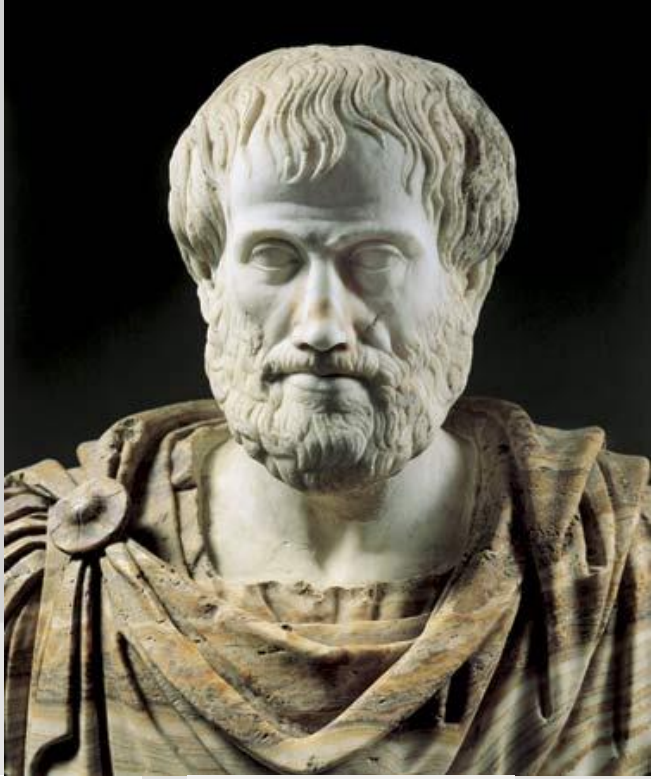

Aristotel
(384 – 322 BC)

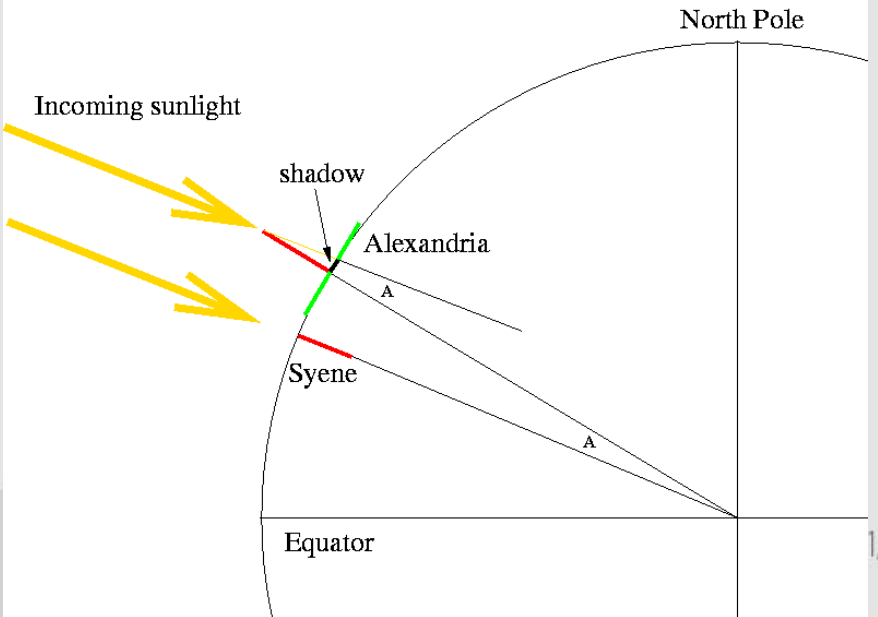

Descoperiri epocale:

- inducţia electromagnetică (M. Faraday – 1831)

- structura atomului (E. Rutherford – 1911)

- structura dublu-helix ADN (J. Watson, F. Crick, M. Wilkins – 1953, Nobel 1962)

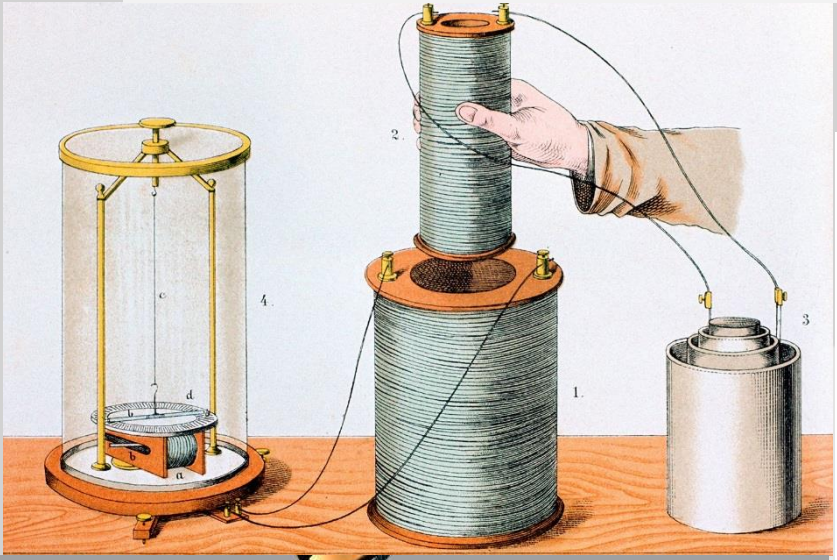

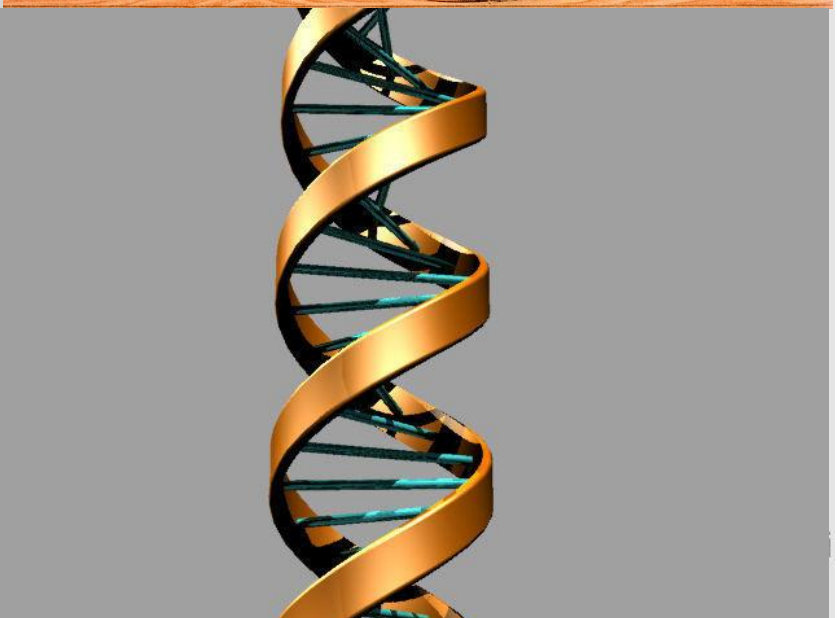

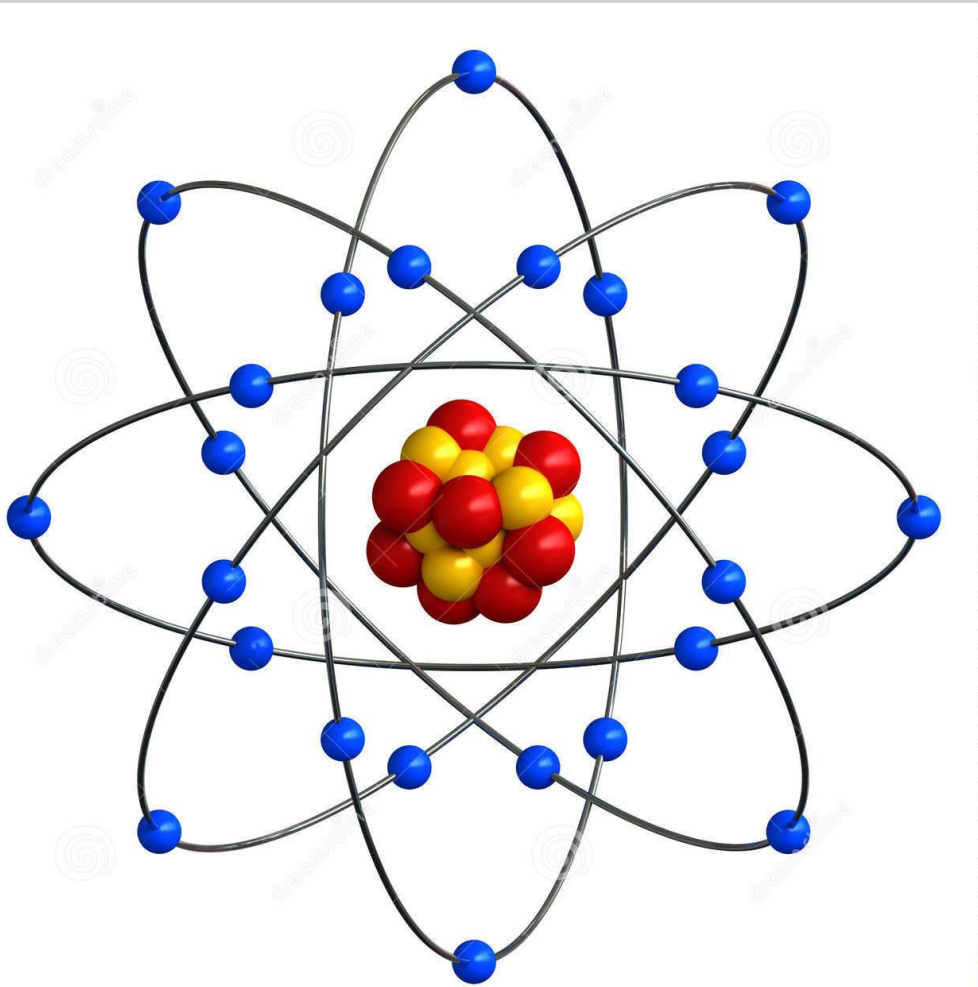

Funcţia formativa:

- dezvoltarea unor aptitudini, competenţe şi abilităţi umane specifice activităţii de cercetare, de promovare a unui mod de gândire şi acţiune specific şi de stimulare a lucrului în echipă, în cadrul unor comunităţi de cercetare locale, naţionale şi internaţionale.

Procesul Bologna

Sistem pentru compatibizarea calificarilor in invatamantul superior din spatial European

- Licenţă
- Masterat
- Doctorat

Echipe de cercetare

Funcţia informativa:

- Stimularea şi întreţinerea interesului opiniei publice şi, în particular, a persoanelor şi instituţiilor capabile şi disponibile să finanţeze cercetări ştiinţifice viitoare.

Diseminare rezultate cercetarii stiintifice:

- articole publicate

- cărţi de specialitate

- brevete de invenţie

- mass media

Diseminarea rezultatelor cercetării ştiinţifice:
- rapoarte de cercetare

www.nature.com/scientificreports

SCIENTIFIC REPORTS

OPEN

Effects of system response delays on elderly humans' cognitive performance in a virtual training scenario

Received: 31 October 2018
Accepted: 23 May 2019
Published online: 05 June 2019

Maria Wirzberger[1,5], René Schmidt[2], Maria Georgi[3,4], Wolfram Hardt[2], Guido Brunnett[4] & Günter Daniel Rey[5]

Observed influences of system response delay in spoken human-machine dialogues are rather ambiguous and mainly focus on perceived system quality. Studies that systematically inspect effects on cognitive performance are still lacking, and effects of individual characteristics are also often neglected. Building on benefits of cognitive training for decelerating cognitive decline, this Wizard-of-Oz study addresses both issues by testing 62 elderly participants in a dialogue-based memory training with a virtual agent. Participants acquired the method of loci with fading instructional guidance and applied it afterward to memorizing and recalling lists of German nouns. System response delays were randomly assigned, and training performance was included as potential mediator. Participants' age, gender, and subscales of affinity for technology (enthusiasm, competence, positive and negative perception of technology) were inspected as potential moderators. The results indicated positive effects on recall performance with higher training performance, female gender, and less negative perception of technology. Additionally, memory retention and facets of affinity for technology moderated increasing system response delays. Participants also provided higher ratings in perceived system quality with higher enthusiasm for technology but reported increasing frustration with a more positive perception of technology. Potential explanations and implications for the design of spoken dialogue systems are discussed.

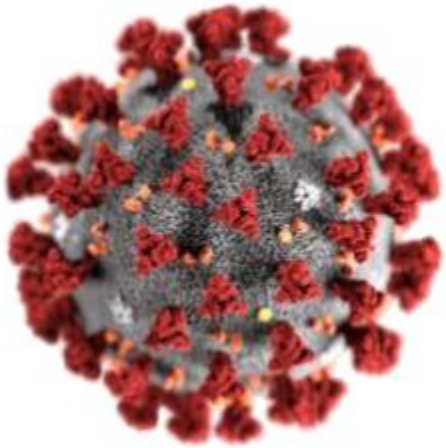

COVID-19 Science Report: Diagnostics

NUS Saw Swee Hock School of Public Health
as of 2200hrs, 19 Mar 2020

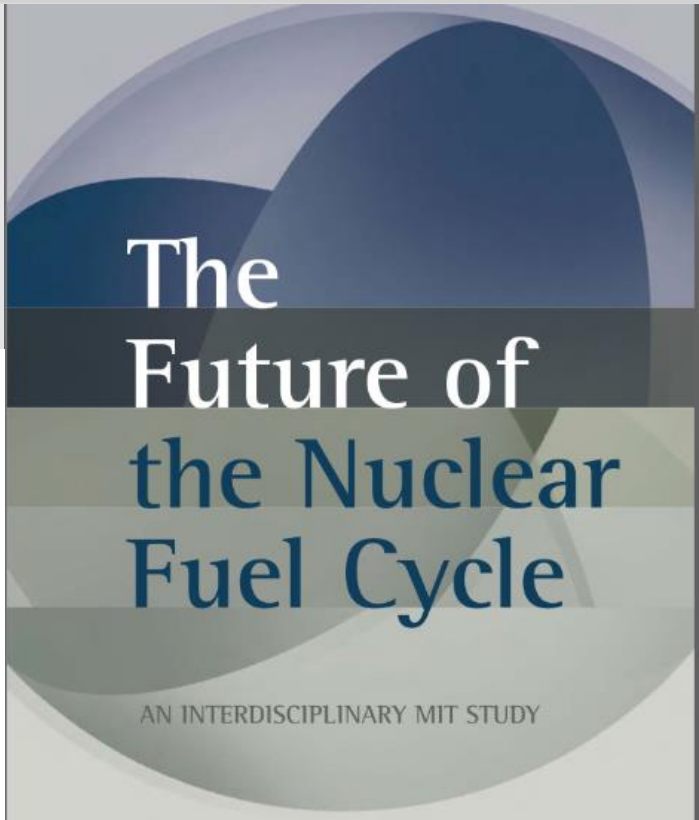

Diseminarea rezultatelor cercetării ştiinţifice:

- comunicări orale

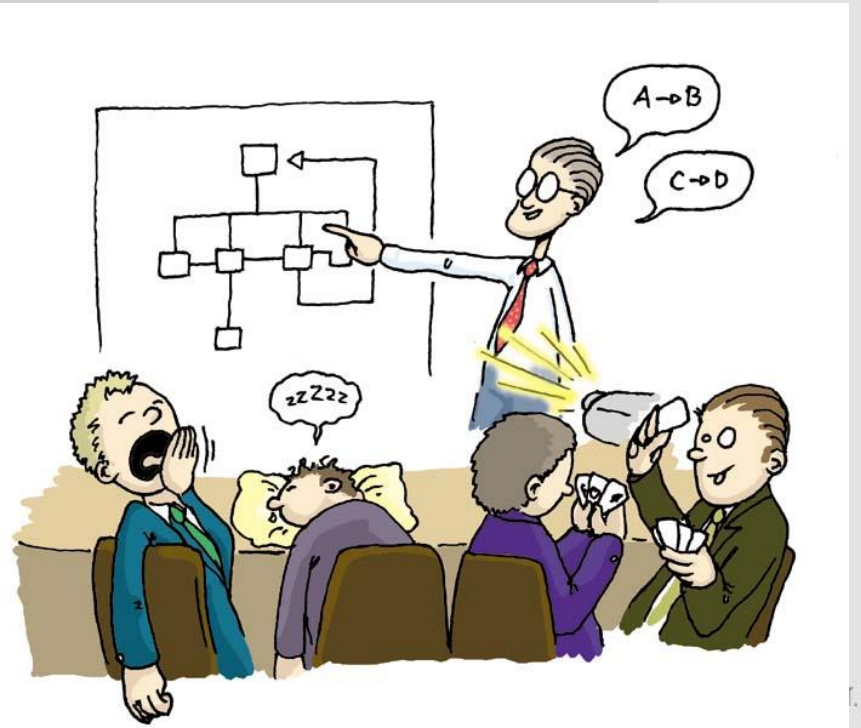

Diseminarea rezultatelor cercetării ştiinţifi

- comunicări poster

STRUCTURA GENERALĂ A UNEI LUCRARI STIINTIFICE

1. Secţiunea de indexare: titlu, autori, aparteneţă, istoric, rezumat, cuvinte cheie, bibliografie

2. Secţiunea de conţinut: introducere, metode experimentale, rezultate, discuţii, concluzii

3. Secţiunea suplimentară: Menţiuni, multumiri

4. Secţiune complementară: Anexe

Clasificarea lucrarilor stiintifice:

- **Lucrare ştiinţifică de sinteză bibliografică (REVIEW)**
- **Lucrare ştiinţifică teoretică**
- **Lucrare ştiinţifică experimentală**

Sinteza bibliografica - recenzii (**Review paper**): O lucrare de recenzie analizează succint progresele recente pe un subiect specific al cercetării active. Ar trebui să rezume starea actuală a cunoașterii subiectului prin discutarea constatărilor prezentate în lucrări de cercetare recente. Lungimea nu trebuie să depășească în mod normal 12000 de cuvinte și 20 de diagrame – aceasta corespunde la aproximativ **18 pagini de jurnal**.

Lucrare ştiinţifică teoretică (**Theoretical paper**) - au ca obiective prioritare dezvoltarea şi aplicarea unor noi idei, metode, modele matematice sau teorii. Ipotezele emise sunt demonstrate matematic sau fenomenologic.

Lucrare ştiinţifică experimentală (**Research papers**): O lucrare de cercetare prezintă rezultatele investigațiilor pe un subiect relevant. Lungimea nu trebuie să depășească în mod normal 8000 de cuvinte și 12 diagrame - aceasta corespunde la aproximativ 12 pagini de jurnal.
Comunicări scurte (**Short communications**): O scurtă comunicare informează comunitatea științifică despre cercetările recente, pe care autorii doresc să le publice cât mai repede posibil, fără a scrie o lucrare de cercetare detaliată. Lungimea nu trebuie să depășească în mod normal 3000 de cuvinte și 4 diagrame - aceasta corespunde la aproximativ 4 pagini de jurnal.

Journal of Power Sources 492 (2021) 229630

Contents lists available at ScienceDirect

Journal of Power Sources

journal homepage: www.elsevier.com/locate/jpowsour

A review of the chemical compatibility between oxide electrodes and electrolytes in solid oxide fuel cells

Linlin Zhang [a], Gang Chen [a,b,*], Ruixin Dai [a], Xiaohong Lv [a], Di Yang [a], Shujiang Geng [a,b]

References

J. Mater. C 9025.
[123] B. Niu, C. Lu, W. Ti, S. Luo, X. Li, X. Zhong, X. Zhao, B. Xu, Appl. Catal. B Environ. 270 (2020), 118842.
[124] X. Mao, T. Yu, G. Ma, J. Alloys Compd. 637 (2015) 286–290.
[125] J. Chen, J. Li, L. Jia, I. Moussa, B. Chi, J. Pu, J. Li, J. Power Sources 428 (2019) 13–19.
[126] T. Chen, Y. Zhou, C. Yuan, M. Liu, X. Meng, Z. Zhan, C. Xia, S. Wang, J. Power Sources 269 (2014) 812–817.
[127] A. Montenegro-Hernández, J. Vega-Castillo, L. Mogni, A. Caneiro, Int. J. Hydrogen Energy 36 (2011) 15704–15714.
[128] E. Yu Pikalova, D.A. Medvedev, A.F. Khasanov, Phys. Solid State 59 (2017) 679–687.
[129] E. Pikalova, A. Kolchugin, N. Bogdanovich, D. Medvedev, J. Lyagaeva, L. Vedmid, M. Ananyev, S. Plaksin, A. Farlenkov, Int. J. Hydrogen Energy 45 (2020) 13612–13624.
[130] X. Chen, J. Wang, Q. Liang, X. Sun, X. Zhu, D. Zhou, J. Meng, Solid State Sci. 100 (2020) 106108.
[131] Q. Zhou, L. Qu, T. Zhang, Y. He, C. Zhao, M. Wang, T. We, Y. Zhang, J. Alloys Compd. (2020), 153967.
[132] C. Ferchaud, J.C. Grenier, Y. Zhang-Steenwinkel, M. van Tuel, F. van Berkel, J. M. Bassat, J. Power Sources 196 (2011) 1872–1879.
[133] H. Nie, T. Wen, S. Wang, Y. Wang, U. Guth, V. Vashook, Solid State Ionics 177 (2006) 1929–1932.
18853–18860.
[165] A. Chen, G. Bourne, K. Siebein, R. DeHoff, E. Wachsman, K. Jones, J. Am. Ceram. Soc. 91 (2008) 2670–2675.
[166] T. Matsui, Y. Mikami, H. Muroyama, K. Eguchi, J. Power Sources 242 (2013) 790–796.
[167] B. Niu, F. Jin, T. Feng, L. Zhang, Y. Zhang, T. He, Electrochim. Acta 270 (2018) 174–182.
[168] J.C. Pérez-Flores, D. Pérez-Coll, S. García-Martín, C. Ritter, G.C. Mather, J. Canales-Vázquez, M. Gálvez-Sánchez, F. García-Alvarado, U. Amador, Chem. Mater. 25 (2013) 2484–2494.
[169] L. Ding, L. Wang, D. Ding, S. Zhang, X. Ding, G. Yuan, J. Power Sources 354 (2017) 26–33.
[170] A. Gómez-Pérez, M.T. Azcondo, M. Yuste, J.C. Pérez-Flores, N. Bonanos, F. Porcher, A. Muñoz-Noval, M. Hoelzel, F. García-Alvarado, U. Amador, J. Mater. Chem. A 4 (2016) 3386–3397.
[171] K.K. Hansen, Fuel Cell. 18 (2018) 96–100.
[172] K. Hansen, K. Hansen, Solid State Ionics 178 (2007) 1379–1384.
[173] K.J. Kim, T.H. Shin, K.T. Lee, J. Alloys Compd. 787 (2019) 1143–1148.
[174] W. Fan, Z. Sun, Y. Bai, K. Wu, Y. Cheng, ACS Appl. Mater. Interfaces 11 (2019) 23168–23179.
[175] O. Celikbilek, C.-A. Thieu, F. Agnese, E. Calì, C. Lenser, N.H. Menzler, J.-W. Son, S.J. Skinner, E. Djurado, J. Mater. Chem. A 7 (2019) 25102–25111.
[176] C. Yang, F. Zhao, F. Chen, M. Liu, Int. J. Hydrogen Energy 39 (2014) 8431–8436.

Physics Open 6 (2021) 100053

Contents lists available at ScienceDirect

Physics Open

journal homepage: www.journals.elsevier.com/physics-open

Quantum simulation of the two-site Hubbard Hamiltonian

Filipe V. Melo *, Alexandre M. Souza, Ivan S. Oliveira, Roberto S. Sarthour

Centro Brasileiro de Pesquisas Físicas, Rua Dr. Xavier Sigaud 150, 22290-180, Rio de Janeiro, Brazil

ARTICLE INFO

ABSTRACT

References

computation, Rev. Mod. Phys. 76 (4) (2005) 1037.

[9] N.A. Gershenfeld, I.L. Chuang, Bulk spin-resonance quantum computation, Science 275 (5298) (1997) 350–356.

[10] J.-S. Lee, The quantum state tomography on an NMR system, Phys. Lett. A 305 (6) (2002) 349–353.

[11] A.M. Souza, G.A. Álvarez, D. Suter, Robust dynamical decoupling for quantum computing and quantum memory, Phys. Rev. Lett. 106 (2011) 240501.

[12] R. Jördens, N. Strohmaier, K. Günter, H. Moritz, T. Esslinger, A Mott insulator of fermionic atoms in an optical lattice, Nature 455 (7210) (2008) 204–207.

[13] S. Murmann, A. Bergschneider, V.M. Klinkhamer, G. Zürn, T. Lompe, S. Jochim, Two fermions in a double well: exploring a fundamental building block of the Hubbard model, Phys. Rev. Lett. 114 (8) (2015), 080402.

[14] M. Steffen, W. van Dam, T. Hogg, G. Breyta, I. Chuang, Experimental implementation of an adiabatic quantum optimization algorithm, Phys. Rev. Lett. 90 (2003), 067903.

Rev. 157 (2) (1967) 295–314.

[21] J.P. Peterson, R.S. Sarthour, R. Laflamme, Enhancing quantum control by improving shaped-pulse generation, Phys. Rev. Appl. 13 (2020), 054060.

[22] N. Khaneja, T. Reiss, C. Kehlet, T. Schulte-Herbrüggen, S.J. Glaser, Optimal control of coupled spin dynamics: design of NMR pulse sequences by gradient ascent algorithms, J. Magn. Reson. 172 (2) (2005) 296–305.

[23] C. Negrevergne, R. Somma, G. Ortiz, E. Knill, R. Laflamme, Liquid-state NMR simulations of quantum many-body problems, Phys. Rev. A 71 (3) (2005), 032344.

[24] X. Yang, A.M. Wang, F. Xu, J. Du, Experimental simulation of a pairing Hamiltonian on an nmr quantum computer, Chem. Phys. Lett. 422 (1–3) (2006) 20–24.

[25] J. Zhang, F.M. Cucchietti, C. Chandrashekar, M. Laforest, C.A. Ryan, M. Ditty, A. Hubbard, J.K. Gamble, R. Laflamme, Direct observation of quantum criticality in ising spin chains, Phys. Rev. A 79 (1) (2009), 012305.

International Journal of Machine Tools & Manufacture 160 (2021) 103672

Contents lists available at ScienceDirect

International Journal of Machine Tools and Manufacture

journal homepage: www.elsevier.com/locate/ijmactool

Characterization of material strain and thermal softening effects in the cutting process

Dong Zhang, Xiao-Ming Zhang *, Guang-Chao Nie, Zheng-Yan Yang, Han Ding

State Key Lab of Digital Manufacturing Equipment and Technology, School of Mechanical Science and Engineering, Huazhong University of Science and Technology, Wuhan 430074, China

ARTICLE INFO

Keywords:
Material constitutive model
Strain softening
Thermal softening
Orthogonal cutting
High-speed filming

ABSTRACT

Accurate descriptions of workpiece behaviors are indispensable for achieving reliable simulations of th cutting process. However, the material plastic constitutive models obtained through conventional materi tests do not apply in the ranges of strain and strain rate encountered in the realistic machining processes. T address this issue, in this study, we attempt to develop a methodology to understand and identify the plasti deformation behaviors based on high-speed filming and induction preheating during the cutting tests. Differen levels of strain, strain rate, and temperature are realized by varying the rake angle, cutting velocity, an initial workpiece temperature, respectively. The plastic deformation and temperature rise in the primary shea zone are characterized by the fine-scale digital image correlation technique and heat convection–conductio equation, respectively, thus rendering the machining test into a high-dynamic-material testing method. Th material exhibits strain softening in the primary shear zone and a reduced thermal softening effect unde rapid heating conditions. These initial findings can deepen the understanding of material behaviors during th cutting process and can be further developed for implementation in numerical machining models.

1. Introduction

Numerical simulations of the metal cutting process are necessary to increase productivity and optimize tool wear [1,2] and surface integrity [3,4]. To apply such approaches, the workpiece behaviors at high plastic strain, strain rate, and temperature as encountered during the cutting process must be determined. However, characterization of the material behaviors under realistic machining conditions is still a challenge because the extremely intense plastic deformation and rapid heating may lead to dynamic recrystallization [5,6] and hinder the microstructure transformation [7], respectively.

The split Hopkinson bar (SHB) tests depicted in Fig. 1(a) have been conventionally adopted to identify the material's constitutive parameters for machining simulation. In the SHB tests, by varying the incident velocity of the incident bar and the heating temperature, compressive tests can be conducted with strain rate and temperature reaching up to several 10^3/s and melting point, respectively.

However, the large strains, high strain rates, and high temperatures concentrated locally in the deformation zones near the cutting tool edge are significantly greater than those achieved by the SHB test. Consequently, extrapolations of the flow stress outside the SHB testing ranges need to be performed. To address the issue of insufficient testing ranges of the SHB, the orthogonal cutting process has been employed as a material test method [8,9] for intense shear deformation in th primary shear zone (PSZ) as illustrated in Fig. 1(b). With the mar developed analytical machining predictive models, the strain, strai rate, temperature, and flow stress along the shear plane (denoted SP in Fig. 1(b)) can be derived using trial material parameters [9–11 Selecting the shear plane for analysis rather than the rear part of th PSZ, which has larger strains, is to simplify the calculation of the she stress through direct decomposition of the measured cutting forc without having to consider the stresses in the secondary or tertia shear zone. Subsequently, the material parameters are tuned until close match is achieved between the calculated and experimental observed quantities, such as cutting forces, shear angles, and cuttin temperatures [12,13]. The comparison of the SHB with the met cutting process as a material test method is presented in Table 1.

The samples commonly used for the SHB tests are cylinders wit a size of a few millimeters, yielding a quasi-homogeneous plast deformation, thus reducing the calculation to a one-dimensional (1I problem. Although the plastic deformation in the through-thickne direction of the workpiece is almost uniform in the case of ortho onal cutting, the thickness of the PSZ is commonly around tens a few hundred micrometers, exaggerating the heterogeneous behai iors of the material microstructure. Consequently, the shear angl of the work material [7]. In this study, we developed an experimental setup for *in situ* severe plastic deformation measurement and rapid workpiece preheating during the orthogonal cutting process to capture the material behaviors, representative of the realistic machining process, as depicted in Fig. 3. The devices used in the experimental tests and their parameters are listed in Table 2.

2.1. Determination of strain and strain rate based on high-speed filming and DIC

To capture the localized high plastic deformation concentrated in the PSZ, a pair of images of the cutting process was captured through a double-shutter camera within a short interframing time of a few micro seconds [27]. Five synchronized high-power green LEDs provided strong illumination of the cutting zone. A maximum strain increment of approximately 0.1 in the PSZ between the captured double images was guaranteed by setting an appropriate interframing time for the double pulses of the lighting; meanwhile, the exposure time of the single pulse of the lighting was selected to be a quarter of the interframing time to obtain a sharp image of the cutting process. A subset with a radius of 37.7 μm was selected, able to provide reasonable spatial resolution during the DIC analysis [28] given the measured thickness of the PSZ, which will be presented in Section 4.1. For the images captured in this study, the zero-mean normalized cross-correlation [29] in the PSZ

* Corresponding author.
E-mail address: chenggxm@hust.edu.cn (X.-M. Zhang).

https://doi.org/10.1016/j.ijmachtools.2020.103672
Received 5 July 2020; Received in revised form 24 November 2020; Accepted 24 November 2020
Available online 27 November 2020

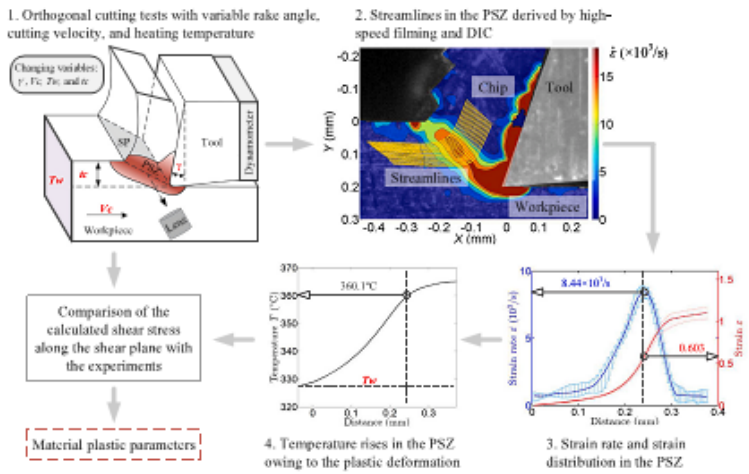

Fig. 2. Flowchart of material testing based on metal cutting process.

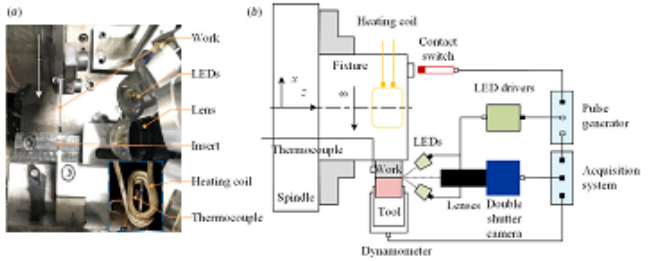

Fig. 3. Material testing based on cutting process, (a) experimental setup and (b) working principle.

Table 2
Descriptions of devices used in the orthogonal cutting tests.

Device	Description
Induction heating	Oscillation frequency ranging from 8 to 100 kHz and an output power of 15 kVA
Thermocouple	*K*-type with a measurement range of 0–1370 °C, and a sampling rate of 10 Hz
High-speed filming	Double-shutter camera with 696 × 520 pixels at 14 bits with a spatial resolution of 3.14 μm/pixel
Optical lens	High-magnification zoom lenses with 4× magnification and a working distance of 87 mm
Illumination lighting	Five green LEDs driven in a pulsed mode with a current of 50 A
Dynamometer	Kistler 9257B with a sampling rate of 10 kHz
Signal synchronizer	Eight independent channel outputs with a resolution of 0.25 ns

Structura unei lucrări ştiinţifice experimentale:

- Titlu
- Autori
- Apartenenţa autorilor
- Abstract
- Keywords
- Introduction
- Experimental part (details)
- Results and discussion
- Conclusions
- Acknowledgement
- References

Cerinţe fundamentale la redactare:
- claritate
- adecvare
- noutate

Universitatea Politehnica Timişoara

Steven Pinker, Simţul stilului – Ghid de scriere pentru oamenii inteligenţi din secolul 21, Editura Publica, 2015.

Steven Pinker, The Sense of Style – The Thinking Persons's Guide to Writing in the 21st Century, Penguin, New York, 2014.

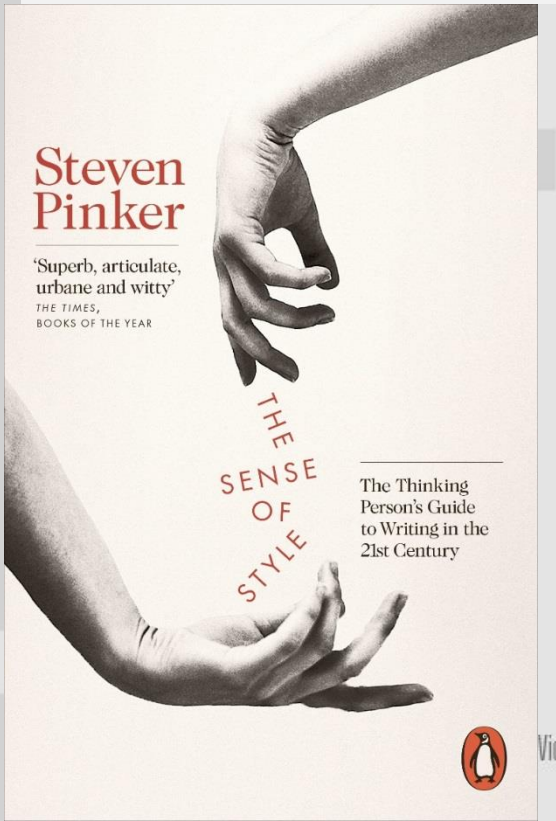

Victoriei nr. 2, RO 300006 - Timişoara, Tel: +

Etica cercetării ştiinţifice:
- proprietarul rezultatelor cercetării ştiinţifice
- recunoaşterea contribuţiilor ştiinţifice
- codul de etică al UPT

Dreptul de autor (copyright): este o formă de proprietate intelectuală care conferă autorului unei lucrări originale priorităţi exclusive pentru o anumită perioadă, referitoare la publicare, distribuţie (comercializare), adaptare (pentru cinematografie sau TV). După această perioadă opera intră în patrimoniul public. Copyrightul are ca scop asigurarea controlului şi profitului pentru autori. In felul acesta este încurajată creaţia ştiinţifică şi artistică.
Durata: 50 – 100 de ani de la moartea autorului.

Plagiatul: însuşirea fără drept a calităţii de autor al unei opere ştiinţifice, literare, muzicale, de artă plastică sau, în general, orice creaţie intelectuală. Noţiunea de plagiat include nu numai însuşirea textului, ci şi a ideilor altui autor, fără a-l cita şi prezentarea lor drept creaţii personale.
Plagiatul reprezintă o infracţiune.

Codul de etica al UPT - Art 37

Pot constitui abateri de la normele de bună conduită în măsura în care nu constituie infracțiuni potrivit legii penale, următoarele fapte descrise de Legea nr. 206/2004:

1. confecţionarea de rezultate sau date şi prezentarea lor ca date experimentale, ca date obţinute prin calcule sau simulări numerice pe calculator ori ca date sau rezultate obţinute prin calcule analitice ori raţionamente deductive;
2. falsificarea de date experimentale, de date obţinute prin calcule sau simulări numerice pe calculator ori de date sau rezultate obţinute prin calcule analitice ori raţionamente deductive;
3. îngreunarea deliberată, împiedicarea sau sabotarea activităţii de cercetare-dezvoltare a altor persoane, inclusiv prin blocarea nejustificată a accesului la spaţiile de cercetare-dezvoltare, prin avarierea, distrugerea ori manipularea aparaturii experimentale, a echipamentului, a documentelor, a programelor de calculator, a datelor în format electronic, a substanţelor organice sau anorganice ori a materiei vii necesare altor persoane pentru derularea, realizarea sau finalizarea activităţilor de cercetare-dezvoltare.
4. plagiatul;
5. autoplagiatul;
6. includerea în lista de autori a unei publicaţii ştiinţifice a unuia sau mai multor coautori care nu au contribuit semnificativ la publicaţie ori excluderea unor coautori care au contribuit semnificativ la publicaţie;
7. includerea în lista de autori a unei publicaţii ştiinţifice a unei persoane fără acordul acesteia;

8. publicarea sau diseminarea neautorizată de către autori a unor rezultate, ipoteze, teorii ori metode ştiinţifice nepublicate;
9. introducerea de informaţii false în solicitările de granturi sau de finanţare, în dosarele de candidatură pentru abilitare, pentru posturi didactice universitare ori pentru posturi de cercetare-dezvoltare,
10. abuzul de autoritate pentru a obţine calitatea de autor sau coautor al publicaţiilor persoanelor din subordine;
11. abuzul de autoritate pentru a obţine salarizare, remunerare sau alte beneficii materiale din proiectele de cercetare-dezvoltare conduse ori coordonate de persoane din subordine;
12. abuzul de autoritate pentru a obţine calitatea de autor sau coautor al publicaţiilor persoanelor din subordine ori pentru a obţine salarizare, remunerare sau alte beneficii materiale pentru soţi, afini ori rude până la gradul al III-lea inclusiv;
13. abuzul de autoritate pentru a impune nejustificat propriile teorii, concepte sau rezultate asupra persoanelor din subordine;
14. obstrucţionarea activităţii unei comisii de etică, a unei comisii de analiză în cursul unei analize a unor abateri de la buna conduită în activitatea de cercetare-dezvoltare din subordine;

Experimental part

Redactarea sectiunii "Experimental part"se face pornind la unul dintre principiile de baze ale elaborarii lucrarilor stiintifice:

Orice lucrare stiintifica trebuie sa poata fi verificata de alti cercetatori,
adica experimentele trebuie sa fie reproductibile, fapt care garanteaza validitatea rezultatelor.

- materialele folosite, indicatori de calitate, furnizori, conditionare si depozitare,
- aspecte teoretice ale metodelor aplicate, formule de calcul, standarde, norme specifice,
- descrierea completa si exacta a echipamentului si a tehnicilor folosite,
- prezentarea in mod exhaustiv a conditiilor de lucru si a operatiilor executate,
- parametrii urmariti experimental,
- modul de prelucrare si interpretare a datelor experimentale, tehnici statistice utilizate,
- informatii asupra soft-urilor folosite (licenta!!!)

Cerinte:
- prezentarea sa fie succinta si clara,
- verbele folosite sa fie la timpul trecut!

Cement and Concrete Research 144 (2021) 106418

Contents lists available at ScienceDirect

Cement and Concrete Research

journal homepage: www.elsevier.com/locate/cemconres

Producing cement clinker assemblages in the system: $CaO-SiO_2-Al_2O_3-SO_3-CaCl_2-MgO$

Marco Simoni [a], Theodore Hanein [a,*], Tristana Y. Duvallet [b], Robert B. Jewell [b], John L. Provis [a], Hajime Kinoshita [a]

[a] University of Sheffield, Department of Materials Science & Engineering, S1 3JD Sheffield, United Kingdom
[b] University of Kentucky Center for Applied Energy Research (UK-CAER), 2540 Research Park Drive, Lexington, KY 40511, USA

ARTICLE INFO

Keywords:
Cement clinker production
Alinite
ye'elimite
Ternesite
Calcium chloride
Industrial circular economy
Low-CO_2

ABSTRACT

The cement industry is carbon-intensive, and the valorisation of industrial side-streams/residuals for use as alternative raw materials can enable the cement industry to reduce its carbon footprint as well as promote resource efficiency. Apart from key clinker ingredients such as CaO, Al_2O_3, and SiO_2, industrial residues can also contain MgO, $CaCl_2$, and SO_3. Therefore, this study investigates the formation of cement clinker assemblages in the system $CaO-SiO_2-Al_2O_3-SO_3-CaCl_2-MgO$ at temperatures ranging between 1100 and 1300 °C. The production of a clinker composed mainly of alinite and ye'elimite is first attempted; it is found that these phases cannot be simultaneously produced. Ternesite is also not compatible with alinite under the conditions studied. Wadalite is compatible with both ye'elimite and ternesite, while ternesite is also compatible with chlormayenite at 1150 °C. Additionally, the low-temperature formation of alite was also observed with the presence of $CaCl_2$ in the raw-material mix.

1. Introduction

1.1. Background

Given the important environmental burden linked to cement manufacture [1], the industry is prioritising the search for low-carbon solutions. Among others, the valorisation of industrial side-streams for use as alternative raw materials and the manufacture of low-energy clinker, are major solutions. Side-streams from industries such as waste-to-energy plants [2,3] and soda ash manufacture [4] contain $CaO-SiO_2-Al_2O_3$ in varying quantities, and can be attractive alternative raw materials for the manufacture of cement clinker as they would reduce the use of CO_2-containing limestone. However, they also comprise significant amounts of $CaCl_2$, MgO, and SO_3 [5,6] in quantities which are unusual for conventional cement kiln raw-meal. Chloride is usually avoided in cements as it can exacerbate the corrosion of mild steel reinforcement in concrete [7]; however, Cl-containing cement clinker can still be employed where steel reinforcement is not utilised or where the Cl is not labile. In addition, more than 60% of cement usage is unreinforced [8]. To enhance industrial circular economy and decarbonisation, it is advantageous to understand clinker phase assemblages in the system: $CaO-SiO_2-Al_2O_3-SO_3-CaCl_2-MgO$.

1.2. Objectives

This study seeks to provide new understanding of the $CaO-SiO_2-Al_2O_3-SO_3-CaCl_2-MgO$ system. Firstly, ye'elimite was targeted as the SO_3-containing phase, whereas alinite was targeted to accommodate $CaCl_2$ and MgO. The separate syntheses of ye'elimite and alinite are first investigated to understand their optimal process conditions for maximum formation. The ye'elemite and alinite produced were then blended in different amounts and fired to assess their co-existence. Then, the co-formation of ye'elemite and alinite in one-step sintering was investigated based on their overlapping formation conditions. The compatibility of alinite and ternesite is also tested and, finally, the co-formation of alinite and chlormayenite is studied with increasing contents of $CaCl_2$.

1.3. Clinker phases of interest

One clinker phase of interest in the system studied here is alinite, a structural variant of tricalcium silicate (alite) [9,10]. This phase is interesting because it can incorporate chloride, magnesium and aluminium as shown in the chemical formula below, proposed by Neubauer et al. [9];

$$Ca_{10}\,Mg_{1-\frac{x}{2}}\,V_{\frac{x}{2}}\,\left[(SiO_4)_{3+x}\,(AlO_4)_{1-x}\right]O_2Cl \quad (1)$$

where the lattice vacancy (V) can be introduced depending on the substitution factor (x). Alinite cement was patented in the USSR in the 1970s and is reported to have been commercially produced by sintering raw materials at 1150 °C [11]. Alinite cements are widely accepted to have comparable mechanical properties to Portland cement (PC) but with faster setting times [9,12]. Table 1 compares the compositions of PC with that of alinite cements, C_3S, and pure alinite produced at a substitution factor of 0.35 (x = 0.35) [9]. As shown in Table 1, significant amounts of chloride and MgO are included in alinite cements; thus, this clinker phase is a good candidate in the $CaO-SiO_2-Al_2O_3-SO_3-CaCl_2-MgO$ system. The presence of chloride salt may also enhance the clinkering reactions by acting as a molten flux [13–16]. Ye'elimite ($C_4A_3\$$), which is the main phase in calcium sulfoaluminate based (CSA) cements, is another clinker phase of interest in the system studied. CSA cements require both a smaller amount of calcium component and a lower production temperature than PC [17]. Considering the compatible formation temperatures of alinite [9,18] and ye'elimite [17], this study explores the feasibility of producing alinite-CSA clinker assemblages. Given the known compatibility issues of alite and ye'elimite under standard processing conditions [19], and the similar cementitious properties of alite and alinite [9,12], the target clinker assemblage may provide an alternative to alite calcium sulfoaluminate (a-CSA) cements that may combine the favourable characteristics of PC and CSA cements [19]. Additionally, certain quantities of MgO in the raw meal have been found to improve the burnability of raw meal and promote the formation of C_3S and $C_4A_3\$$ in a-CSA cements [20,21].

2. Materials and methods

2.1. Materials

Raw mixtures were prepared from reagent grade chemicals: $CaCO_3$ (≥99%, Acros Organics), $CaSO_4$ (99%, Acros Organics), SiO_2 (99.5% Alfa Aesar), Al_2O_3 (≥99%, Acros Organics), $CaCl_2$ (96%, Acros Organics), and MgO (≥99.5%, Strem Chemicals Inc.).

2.2. Analysis techniques

X-ray diffraction (XRD) patterns were collected using a Panalytical X'Pert Pro PW3040 operating in reflection mode with Cu-Kα radiation (45 kV, 40 mA) and a diffracted beam monochromator (5.5 mm), at a scanning speed of 0.013° per second. All samples were backloaded, and measurements were conducted without rotation. Rietveld quantitative analysis was performed using Highscore plus (database PDF^{-4}2019) for all the samples, and the diffraction patterns used as a reference (Table 2) were from ICDD (International Centre for Diffraction Data) files.

Apart from a good match between the measured and calculated Rietveld patterns, R_{wp} (weighted pattern residual error) and GOF (goodness of fit) values [39] below 10.0% and 5.0% respectively were required for reliable results [40]. To validate the Rietveld analysis, opportune calculations were performed. Firstly, by retro-calculation from Rietveld quantification, the weight losses $\Delta wt\%_{(R)}$ were obtained as a sum of CO_2 ($\Delta wt\%CO_{2(R)}$), $CaCl_2$ ($\Delta wt\%CaCl_{2(R)}$) and SO_3 ($\Delta wt\%SO_{3(R)}$) losses; the difference between the experimental weight losses $\Delta wt\%_{(Exp)}$ and the calculated $\Delta wt\%_{(R)}$ was expressed as $\Delta wt\%_{(Exp-R)}$ and are reported in the Appendix. Furthermore, all the weight compositions were normalised only in terms of CaO (C), Al_2O_3 (A) and SiO_2 (S); the respective input/output differences ΔC, ΔA and ΔS (Appendix) would also allow for the evaluation of the Rietveld analyses. The lower the ΔC, ΔA, and ΔS values, the more reliable the solid phase quantification is. While MgO was not taken into account for this calculation because of its small content, both $CaCl_2$ and SO_3 were also excluded from this mass balance since they were volatile.

Simultaneous DSC/TG (SDT) analysis was performed on 20–40 mg of powder samples in a SDT Q600 (TA Instruments) instrument, operating between 50 °C and 1400 °C in an air atmosphere (flow rate 100 mL/min) at a heating rate of 10 °C/min; the samples were placed in disposable alumina crucibles for measurement.

Table 1
Oxide compositions (wt%) of PC, alinite-based cements, and alinite (x = 0.35) with general formula: $Ca_{10}\,Mg_{(1-x/2)}\,V_{(x/2)}\,[(SiO_4)_{(3+x)}\,(AlO_4)_{(1-x)}]\,O_2Cl$.

	PC [22]	Commercial alinite cement [11]	Other alinite cements [18,23]	Pure alinite (x = 0.35) [9]	Stoichiometric alite (C_3S)
CaO	67	45–55	45–61	62	74
SiO_2	22	13–19	13–21	24	26
Al_2O_3	5	9–12	2–12	4	–
Fe_2O_3	3	4–10	2–10	–	–
MgO	<3	1–10	1–10	4	–
$CaCl_2$	–	6–18	4–18	6	–

2.3. Clinkering procedure

To ensure homogeneity, all the samples were prepared by blending the pre-dried powders for 5 min using a Rocklabs BenchTop Ring Mill (Scott products) within a Carbon/Chrome 100 head. Powders were then pelletised by applying a pressure of 11 atm; ~2 cm diameter and ~0.5 cm height pellets were obtained. All the pellets were placed in platinum crucibles and pre-heated at 150 °C for 30 min prior to firing. Preliminary experiments highlighted a lower efficiency in the synthesis of alinite when a ramp temperature program was used compared to when samples were inserted at target temperature; the gradual temperature increase led to increased volatilisation of $CaCl_2$. Since alinite was a main target phase, no ramp was used in clinkering. This method also enabled avoiding formation of any phases that are stable at a lower temperature, and that may then persist after heating; in this way, only phases stable at the target temperature will be observed. In all experiments, samples were fired once only at target temperature and only one sample was produced for each experiment using a consistent methodology.

All sintered products were cooled in air (fan-assisted) at room temperature before grinding and sieved below 75 μm for XRD analysis. The individual production of alinite was tested under different conditions aiming for a maximum conversion; two procedures were tested. The first method was based on the setup of Neubauer and Pöllmann [9] where the pellet was reacted in a sealed system. This was mimicked by using a sealed ceramic outer vessel with a total volume of 40 mL. The sealed system was provided with an extra source of $CaCl_2$, external to the sample, which was ~5 times the amount present in the reacting solid blend; this provided a $CaCl_2$-rich atmosphere within the system, inhibiting $CaCl_2$ escape from the raw-material mixture. In the second method, similar to that used by Vaidyanathan et al. [18], excess $CaCl_2$ was used directly within the raw-material mixture. Both studies [9,18] indicated optimal sintering conditions of 1150 °C for 5 h; in the present study, experiments were carried out at various temperatures and times as detailed in the following sections.

To investigate the possibility of single-stage manufacture of clinker containing both alinite and ye'elimite, the conditions allowing for the individual optimal production of each phase was tested. Variations in temperature and sintering time were investigated, and the conditions allowing for the maximum conversions were detected. Then, the phases produced from these tests were used as raw materials in a second stage of experiments, to study their co-existence upon re-firing. The co-

* Corresponding author.
E-mail address: t.hanein@sheffield.ac.uk (T. Hanein).

https://doi.org/10.1016/j.cemconres.2021.106418
Received 27 May 2020; Received in revised form 24 February 2021; Accepted 26 February 2021
Available online 8 March 2021
0008-8846/

2. Materials and methods

2.1. Materials

Raw mixtures were prepared from reagent grade chemicals: $CaCO_3$ (≥99%, Acros Organics), $CaSO_4$ (99%, Acros Organics), SiO_2 (99.5% Alfa Aesar), Al_2O_3 (≥99%, Acros Organics), $CaCl_2$ (96%, Acros Organics), and MgO (≥99.5%, Strem Chemicals Inc.).

2.2. Analysis techniques

X-ray diffraction (XRD) patterns were collected using a Panalytical X'Pert Pro PW3040 operating in reflection mode with Cu-Kα radiation (45 kV, 40 mA) and a diffracted beam monochromator (5.5 mm), at a scanning speed of 0.013° per second. All samples were backloaded, and measurements were conducted without rotation. Rietveld quantitative analysis was performed using Highscore plus (database PDF^{-4}2019) for

2.3. Clinkering procedure

To ensure homogeneity, all the samples were prepared by blending the pre-dried powders for 5 min using a Rocklabs BenchTop Ring Mill (Scott products) within a Carbon/Chrome 100 head. Powders were then pelletised by applying a pressure of 11 atm; ~2 cm diameter and ~0.5 cm height pellets were obtained. All the pellets were placed in platinum crucibles and pre-heated at 150 °C for 30 min prior to firing. Preliminary experiments highlighted a lower efficiency in the synthesis of alinite when a ramp temperature program was used compared to when samples were inserted at target temperature; the gradual temperature increase led to increased volatilisation of $CaCl_2$. Since alinite was a main target phase, no ramp was used in clinkering. This method also enabled avoiding formation of any phases that are stable at a lower temperature, and that may then persist after heating; in this way, only phases stable at the target temperature will be observed. In all experiments, samples were fired once only at target temperature and only one sample was produced for each experiment using a consistent methodology.

All sintered products were cooled in air (fan-assisted) at room temperature before grinding and sieved below 75 μm for XRD analysis. The individual production of alinite was tested under different conditions aiming for a maximum conversion; two procedures were tested. The first method was based on the setup of Neubauer and Pöllmann [9] where the pellet was reacted in a sealed system. This was mimicked by using a sealed ceramic outer vessel with a total volume of 40 mL. The sealed system was provided with an extra source of $CaCl_2$, external to the sample, which was ~5 times the amount present in the reacting solid blend; this provided a $CaCl_2$-rich atmosphere within the system, inhibiting $CaCl_2$ escape from the raw-material mixture. In the second method, similar to that used by Vaidyanathan et al. [18], excess $CaCl_2$ was used directly within the raw-material mixture. Both studies [9,18] indicated optimal sintering conditions of 1150 °C for 5 h; in the present study, experiments were carried out at various temperatures and times as detailed in the following sections.

To investigate the possibility of single-stage manufacture of clinker containing both alinite and ye'elimite, the conditions allowing for the individual optimal production of each phase was tested. Variations in temperature and sintering time were investigated, and the conditions allowing for the maximum conversions were detected. Then, the phases produced from these tests were used as raw materials in a second stage of experiments, to study their co-existence upon re-firing. The co-

Corrosion Science 184 (2021) 109350

Contents lists available at ScienceDirect

Corrosion Science

journal homepage: www.elsevier.com/locate/corsci

Corrosion of SS310 and Alloy 740 in high temperature supercritical CO_2 with impurities H_2O and O_2

Kaiyang Li [a], Yimin Zeng [b,*], Jing-Li Luo [a,*]

[a] Department of Chemical and Materials Engineering, University of Alberta, Edmonton, Albe
[b] Natural Resources Canada, CanmetMATERIALS, Hamilton, Ontario, L8P 0A5, Canada

2. Experimental details

2.1. Test sample preparation

Flat test samples (20 mm long ×10 mm wide ×2 mm thick) were machined from commercial SS310 and Alloy 740 plates, and their normalized chemical compositions are shown in Table 1. A small hole (2 mm in radius) was made near the top middle of each coupon for suspending on a custom holder during high-temperature s−CO_2 exposure. Before autoclave testing, all the coupons were well polished with SiC papers up to 600 grit finish, cleaned with distilled water, degreased with ethanol in an ultrasonic bath, and dried by compressed air. Optical microscopy inspection was then conducted to determine whether the surface finish of each coupon met the standard requirements. Following that, the coupons were weighed using a microbalance with a resolution of 1 μg and dimensioned using a digital caliper with a precision of 10 μm.

2.3. Corrosion rate assessments and corrosion product characterizations

The corrosion rates of two alloys were assessed based on two different methods: (1) direct mass change measurements and (2) mass loss measurements. For the first method, the direct mass change of each alloy coupon was weighed before the corrosion testing and after exposure. The coupon with the mass change closest to the average value from four replicates was selected for further corrosion product characterization. The mass loss method involves descaling the formed surface corrosion products and acquiring the mass change of each coupon before testing and after descaling treatment. Based on ASTM G1-03 [33], the corroded coupons were immersed in solution A (4% $KMnO_4$ + 2% NaOH) at 90 °C for 5 min, and then in solution B (2% citric acid+ 5% dibasic ammonium citrate + 0.5 % disodium EDTA) at 90 °C for 30 min. After each immersion, the coupons were ultrasonically cleaned in alcohol. Alternative immersions in solutions A and B were repeated until the mass of the coupon reached a constant value. The corrosion rate (in μm/y) of each coupon was then evaluated by [34]:

$$\text{Corr.rate} = \frac{8.76 \times 10^4 \times \Delta W}{A\rho t} \quad (1)$$

Results and discussion

Universitatea Politehnica Timişoara

Este sectiunea in care sunt anuntate descoperirile autorilor

Sunt prezentate datele obtinute de autori sub forma de:
- tabele,
- grafice,
- diagrame.
Se vor evita redundantele in prezentare.

In mod obligatoriu se includ si rezultatele negative.

Be sure to include negative results –
writing a results section without them not only invalidate the paper,
but it is extremely bad science.

Unitati de masura - Sistemul International de Unitati

- Unitati fundamentale

Fundamental Quantities	SI Unit	Symbol
Length	meter	m
Mass	kilogram	kg
Time	second	s
Electric current	Ampere	A
Temperature	Kelvin	K
Amount of subtance	mol	mol
Luminous Intensity	candela	cd

Unitati derivate

Physical Quantity	Symbol	Name and Symbol SI Unit	Fundamental Units Involved	Derived Units involved
frequency	f or ν	hertz (Hz)	s^{-1}	s^{-1}
force	F	newton (N)	kg m s^{-2}	kg m s^{-2}
work	W	joule (J)	kg m^2 s^{-2}	Nm
energy	Q, Ep, Ek, Eelas	joule (J)	kg m^2 s^{-2}	Nm
power	P	watt (W)	kg m^2 s^{-3}	J s^{-1}
pressure	P	pascal (Pa)	kg m^{-1} s^{-2}	N m^{-2}
charge	Q	coulomb (C)	A s	A s
potential difference	V	volt (V)	kg m^2 s^{-3} A^{-1}	J C^{-1}
resistance	R	ohm (Ω)	kg m^2 s^{-3} A^{-2}	V A^{-1}
magnetic field intensity	B	tesla (T)	kgs^{-3} A^{-1}	NA^{-1} m^{-1}
magnetic flux	Φ	weber (Wb)	kg m^2 s^{-2} A^{-2}	T m^2
activity	A	becquerel (Bq)	s^{-1}	s^{-1}
absorbed dose	W/m	gray (Gy)	m^2 s^{-2}	J kg^{-1}

Figure 103 Derived Units

Prefixe pentru unitati

Prefix	Symbol for Prefix		Scientific Notation
exa	E	1 000 000 000 000 000 000	10^{18}
peta	P	1 000 000 000 000 000	10^{15}
tera	T	1 000 000 000 000	10^{12}
giga	G	1 000 000 000	10^{9}
mega	M	1 000 000	10^{6}
kilo	k	1 000	10^{3}
hecto	h	100	10^{2}
deka	da	10	10^{1}
----	--	1	10^{0}
deci	d	0.1	10^{-1}
centi	c	0.01	10^{-2}
milli	m	0.001	10^{-3}
micro	μ	0.000 001	10^{-6}
nano	n	0.000 000 001	10^{-9}
pico	p	0.000 000 000 001	10^{-12}
femto	f	0.000 000 000 000 001	10^{-15}
atto	a	0.000 000 000 000 000 001	10^{-18}

Universitatea Politehnica Timişoara

Atentie la prezentarea valorilor numerice: cifre semnificative!!!

$0.3452756489\ V \rightarrow 0.3453\ V \rightarrow 0.345\ V$

$pH = 7.67895 \rightarrow pH = 7.68 \rightarrow pH = 7.7$

$0.000000123\ m \rightarrow 0.123 \cdot 10^{-6}\ m \rightarrow 1.23 \cdot 10^{-7}\ m$

Prezentarea unitatilor de masura

$\frac{kg \cdot m}{s^2}$ $kg\ m\ s^{-2}$

Notatii si abrevieri

Temperatura: *t* *T*

Energie: *E* *W*

Curent: *I* *i*

SEM – scanning electronic microscopy;
TEM – transmission electronic microscopy,
DNA – dezoxiribinucleic acid,
NMR – nuclear magnetic resonance

Corrosion Science 69 (2013) 389–395

Contents lists available at SciVerse ScienceDirect

Corrosion Science

journal homepage: www.elsevier.com/locate/corsci

Corrosion resistance of carbon steel in weak acid solutions in the of L-histidine as corrosion inhibitor

Marian Bobina [a], Andrea Kellenberger [a], Jean-Pièrre Millet [b], Cornelia Muntean [a], Nico

[a] University Politehnica of Timisoara, Piata Victoriei 2, 300006 Timisoara, Romania
[b] University of Lyon, INSA-Lyon, MATEIS – CNRS UMR 5510, F69621 Villeurbanne Cedex, France

ARTICLE INFO

Article history:
Received 25 July 2012
Accepted 19 December 2012
Available online 11 January 2013

Keywords:
L-histidine
Corrosion inhibitor
Inhibition efficiency
Electrochemical impedance spectroscopy

ABSTRACT

This paper presents the inhibitory properties of L-histidine on the corrosi media containing acetic acid/sodium acetate. The inhibition efficiencies surements are in good agreement with values given by Tafel method a spectroscopy. The adsorption of L-histidine obeys the Langmuir isotherm a energy indicate the nature of interactions between inhibitor molecules a inhibition effect was studied using scanning electron microscopy and en

1. Introduction

The use of chemical compounds in a very wide range of applications is restricted by the protection of the environment and health considerations. Lately, at industrial level, it was required to use chemicals not only due to their efficiency, but also to their safety. These concepts are valid as well in the field of organic compounds which act as corrosion inhibitors for metals and alloys. In this respect, there is a special emphasis on natural compounds, nontoxic and ecologically friendly. In this way, berberine [1], tryptamine [2] and some extracts from natural plants [3–6] were reported as efficient corrosion inhibitors for steel and iron in different test solutions. The amino acids and derivatives have been used as good corrosion inhibitors for mild steel [7–12], carbon steel [13–15], stainless steel [16], iron [17], nickel [18], copper [19,20], aluminum [21], and alloys [22,23] in different aggressive solutions.

Generally, these compounds act on the corrosion process by adsorption on the metal surface, forming a protective film and blocking the active sites. The adsorption mechanism of the inhibitor molecules plays a very important role because the protection degree of the metal or alloy depends on the adsorption process [16].

The aim of this work is to investigate the inhibiting properties of L-histidine on the corrosion process of carbon steel in corrosive solutions containing sodium acetate, the main ingredient used in deicing solutions [24], and acetic acid in order to ensure a constant pH and more aggressive media. Sodium acetate, either liquid or solid, is effective at low temperature in ice and deep snow [24], and has been used on some winter roadwa salts, being less corrosive and more su [25]. Ice Shear is an improved deicing n acetate and sodium formate which exh freezing point of water, penetrate ice bonding between the ice and paveme deicers with an ecological corrosion i taking into account that this kind of sol e.g. highways, airplanes and airports,

Studies on the corrosion process o solutions are of industrial importanc boxyl group makes them a basic bui pounds such as drugs, pharmaceuticals

It is required to mention that L-hi corrosion inhibitor for mild steel as we tions [7].

2. Experimental

The weight loss, linear polarization, spectroscopy and cyclic voltammetry to observed the inhibitive properties o process. The surface morphology of th investigated after removing the produ tack. The adsorption isotherm of the studied and discussed.

2.1. Materials

The chemical structure of L-histidin

* Corresponding author. Tel.: +40 256404180.
E-mail address: nicolae.vaszilcsin@chim.upt.ro (N. Vaszilcsin).

0010-938X/$ - see front matter © 2013 Elsevier Ltd. All rights reserved.
http://dx.doi.org/10.1016/j.corsci.2012.12.020

Table 1
Elemental composition of the carbon steel samples.

Element	Fe	C	Si	Mn	P	S	Cr	Ni
wt.%	96.98	0.4184	0.2510	0.7920	0.0132	0.0335	1.162	0.029
Element	Mo	Cu	Al	Ti	V	Co	Nb	W
wt.%	0.2123	0.0234	0.0229	<0.004	0.0124	0.0222	<0.001	<0.010

Experimental measurements were carried out on cylindrical samples of carbon steel with the elemental composition presented in Table 1.

Different concentrations of the inhibitor, L-histidine (Merck, 99%), between 10^{-4} and 10^{-2} M, have been used to determine the inhibition effect of this amino acid on the corrosion rate of carbon steel in 0.5 M CH_3COOH/0.25 M CH_3COONa test solutions. The corrosive media was prepared from glacial acetic acid (Fluka, 99.8%) and sodium acetate (Fluka, 99%).

2.2. Weight loss measurements

Weigh loss (W) experiments were carried out using disc samples of carbon steel having the dimensions Φ 15 mm × 5 mm. Before immersion in the test solutions with or without the inhibitor, the samples were abraded with different SiC paper (220, 500, 800, and 1000), ultrasonically cleaned in distilled water, rinsed with acetone and finally dried. After 240 h exposure time at room temperature in 100 mL corrosive solutions, the specimens were taken out, brushed under running water to remove the corrosion products, washed with distilled water and acetone and dried. Before and after the corrosive attack the samples have been weighed using an analytical balance (precision ±0.1 mg). The weight loss in mg cm^{-2} h^{-1} has been calculated using Eq. (1) [29]:

$$W = \frac{W_1 - W_2}{S \times t} \quad (1)$$

where W_1 and W_2 are the initial and final mass of the samples in mg, S is the total surface area of specimens in cm^2 and t is the exposure time in h.

From the calculated W the inhibition efficiency (η) and surface coverage (θ) of the inhibitor were obtained using Eqs. (2) and (3) [30]:

$$\eta(\%) = \left(1 - \frac{W_{corr}}{W^o_{corr}}\right) \times 100 \quad (2)$$

$$\theta = 1 - \frac{W_{corr}}{W^o_{corr}} \quad (3)$$

where W_{corr} and W^o_{corr} are the weight loss of the samples in the presence and absence of the inhibitor, respectively.

2.3. Electrochemical measurements

Potentiodynamic polarization measurements were carried out in 0.5 M CH_3COOH/0.25 M CH_3COONa test solutions in the absence and presence of different concentrations (10^{-4}–10^{-2} M) of L-histidine, in a conventional three-electrodes cell at room temperature. Carbon steel samples with 1 cm^2 surface area in contact with solution were used as working electrodes, the reference was a silver–silver chloride electrode (Ag/AgCl/saturated KCl) and two graphite rods were used as counter electrodes. The samples preparation before the experiments was similar to weight loss measurements. Before each experiment the test solutions were deaerated by bubbling high purity nitrogen in order to avoid any reaction with dissolved oxygen. Polarization curves were obtained with an Autolab PGSTAT 302N at a scan rate of 2 mV s^{-1} in the potential range of −200 mV to +200 mV relative to the open circuit potential. Electrochemical impedance spectroscopy (EIS) measurements were carried out at E_{corr} at 298 ± 1 K after a stationary state was achieved in the frequency range from 10 kHz to 10 mHz and AC voltage amplitude of 10 mV peak to peak. The EIS spectra were measured in a three electrodes cell connected to a PAR 2263 potentiostat. The working electrode was carbon steel with an active surface of 0.5 cm^2, the counter electrode was a Pt wire and the reference a saturated calomel electrode. Before each experiment the surface of the electrode was prepared similarly as previously described and the test solutions were deaerated by bubbling pure nitrogen for 1 h.

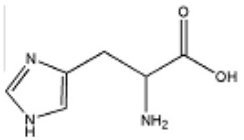

Fig. 1. Chemical structure of L-histidine.

2.4. Surface morphology

Carbon steel surface was analyzed with a Keyence VHX-600 Digital Microscope and a Philips XL 30 ESEM scanning electron microscope (SEM), respectively. The images of the samples, same used in the weight loss measurements, were recorded after 240 h exposure time in test solutions in the absence and the presence of L-histidine.

3. Results and discussion

3.1. Weight loss data

From the weight loss data of carbon steel samples after 240 h immersion time in corrosive solutions, in the absence and presence of different amounts of L-histidine, the inhibition efficiency and surface coverage were calculated and the results are given in Table 2. The results indicate that amino acid reduces the corrosion process and the effect is more pronounced as the concentration of the inhibitor increases.

Table 2
The inhibition efficiency and surface coverage obtained by weight loss measurements.

L-histidine conc. (M)	η (%)	θ (surface coverage)
1×10^{-4}	31.9	0.319
5×10^{-4}	44.5	0.445
1×10^{-3}	58.2	0.582
5×10^{-3}	68.7	0.687
1×10^{-2}	81.6	0.816

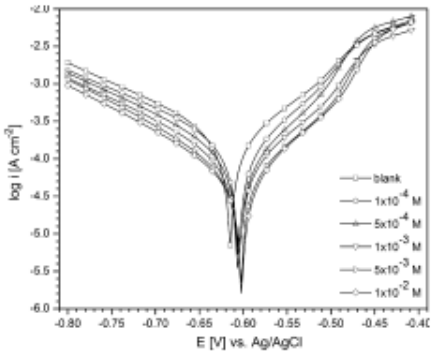

Fig. 2. Linear polarization curves on carbon steel electrode in 0.5 M CH_3COOH/0.25 M CH_3COONa with and without various concentrations of L-histidine.

3.2. Linear polarization

One of the most used methods to determine the corrosion rate of metals and alloys in corrosive solutions is linear polarization. Fig. 2 reveals the cathodic and anodic polarization curves obtained for carbon steel in 0.5 M CH_3COOH/0.25 M CH_3COONa at room temperature in the absence and presence of different concentrations of L-histidine.

The values of electrochemical parameters associated with this process, i.e. corrosion potential (E_{corr}), corrosion current density (i_{corr}), cathodic and anodic Tafel slopes (b_c and b_a) and corrosion rate were determined by extrapolating potentiodynamic curves using GPES software. Also, the inhibition efficiency (η) and surface coverage have been calculated with Eqs. (4) and (5) [31] and the values obtained are presented in Table 3.

$$\eta(\%) = \left(\frac{i_{corr} - i^{o}_{corr}}{i_{corr}}\right) \times 100 \quad (4)$$

$$\theta = \frac{i_{corr} - i^{o}_{corr}}{i_{corr}} \quad (5)$$

where i_{corr} and i^{o}_{corr} are the uninhibited and inhibited corrosion current densities, respectively.

The analysis of data given in Table 3 shows that both the cathodic and anodic Tafel slopes decrease indicating that L-histidine is a mixed type inhibitor acting on both the hydrogen evolution reaction and metal dissolution. Moreover, the Tafel slopes do not suffer significant variation with increase of amino acid concentration suggesting that the presence of inhibitor in the test solution does not modify the process mechanism and act as adsorptive inhibitor, retarding both cathodic and anodic reaction by blocking the active sites [17,32]. An increase in inhibitor concentration probably increase the number of inhibitor
interface and decrease the corro
the corrosion potential value slig
The inhibition process can be att
L-histidine molecules on the activ
sition of corrosion products on th

From the Tafel polarization res
inhibition mechanism involves bl
the inhibitor molecules via adsor

3.3. EIS measurements

Information about the inhibiti
also obtained by electrochemic
advantage of this method is that
values also double layer capacita
same measurement.

Fig. 3 gives the EIS spectra of
without and with various concen

The complex plane plots revea
pressed semicircle. The diameter
the polarization resistance and it
of L-histidine.

A simple electrical equivalent
to model the experimental data.
nection between the solution res
tion of the double layer capac
resistance. Due to the deviations f
itance is usually replaced by a
whose impedance is given by:

$$Z_{CPE} = 1/T(j\omega)^{n}$$

where T is a parameter related to t
is an exponent between 0 and 1 de
of the CPE.

The experimental data were fit
linear least-squares (CNLSs) proc
ues of the circuit elements are gi
standard errors.

The inhibition efficiency was
resistance values using Eq. (7) [3

$$\eta(\%) = \left(\frac{R_{p,inh} - R_p}{R_{p,inh}}\right) \times 100$$

where $R_{p,inh}$ and R_p are polarizati
ence and absence of L-histidine.

The obtained values of the in
the concentration of amino acid
the values calculated from linea
weight loss measurements.

Double layer capacitance value
impedance data using Eq. (8) and

$$T = C^{n}_{dl}\left(R_s^{-1} + R_p^{-1}\right)^{1-n}$$

Table 3
Polarization parameters for the corrosion of carbon steel in 0.5 M CH_3COOH/0.25 M CH_3COONa with/without various concentration

Inh. conc. (M)	i_{corr} (μA cm^{-2})	$-E_{corr}$ (mV)	$-b_c$ (mV dec^{-1})	b_a (mV dec^{-1})	R_p (Ω)	Corr. ra
Blank	159.0	615	168	118	44.3	1.87
1 × 10^{-4}	114.1	605	165	102	64.1	1.34
5 × 10^{-4}	89.3	605	155	102	76.1	1.05
1 × 10^{-3}	70.1	605	152	102	96.5	0.82
5 × 10^{-3}	52.2	603	142	95	121.8	0.61
1 × 10^{-2}	33.1	601	141	87	148.7	0.48

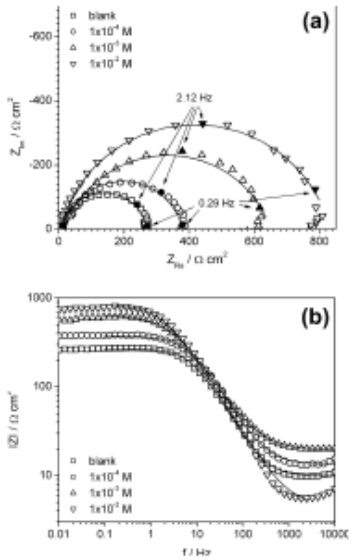

Fig. 3. Experimental Nyquist (a) and Bode (b) plots of carbon steel in 0.5 M CH_3COOH/0.25 M CH_3COONa with and without various concentrations of L-histidine. Symbols are experimental data and continuous lines are obtained by CNLS fitting.

It can be observed that the double layer capacitance in the absence of inhibitor is larger than in its presence. The addition of L-histidine in the test solution leads to a decrease of the double layer capacitances, because the inhibitor molecules adsorb at the inner Helmholtz plane and block the active sites on the metal surface.

3.4. Cyclic voltammetry

The manner in which L-histidine can influence the corrosion process is pointed by its electrochemical behavior in test solutions studied by cyclic voltammetry. Fig. 4 shows the cyclic voltammograms recorded in 0.5 M CH_3COOH/0.25 M CH_3COONa on platinum electrode in the absence and the presence of different amounts of inhibitor. On the base curve, in the absence of L-histidine, the anodic branch corresponding to the oxygen release (curve 1) and the cathodic one for hydrogen evolution reaction (curve 2) are distinctive. Further, one can also observe the reduction peak (3) of the oxide layer formed on electrode surface and the peak (4) associated with the oxidation of adsorbed hydrogen. The addition of compound in the test solution leads to an increase of the current (5) that can be attributed to amino acid oxidation. Also, the presence of inhibitor in the test solution reduces the cathodic and anodic processes.

The cyclic voltammograms measured on carbon steel electrode in the same test solutions in the absence and the presence of L-histidine is presented in Fig. 5. The main curve shows, along the oxygen and hydrogen evolution reactions (2 and 6), the characteristic peaks for metal dissolution (1 and 4). On the cathodic branch, one can observe the reduction current (peak 3) corresponding to the reduction of the passive film and the current plateau 5 attributed to the reduction of iron ions to metallic iron. Also, in the anodic sense, peak 7, corresponding to the oxidation of adsorbed hydrogen on metal surface, is observed.

In the presence of the amino acid in the test solution, the passivation of the metal surface occurs more easily, critical current being reduced.

3.5. Adsorption isotherm

Useful information about the inhibition mechanism of carbon steel corrosion process can be gained from adsorption isotherm, by determining the standard Gibbs free energy value that characterizes the type of interaction existing between inhibitor molecules and metal surface. The Gibbs energy was calculated with Eq. (9) [35].

$$\Delta G^{o}_{ads} = -RT\ln(55.5K_{ads}) \quad (9)$$

where R is the universal gas constant 8.314 J mol^{-1} K^{-1}, T the thermodynamic temperature in K, K_{ads} is the equilibrium constant for the adsorption process and 55.5 represents the molar concentration of water in the solution.

In the case of amino acids adsorption the most suitable isotherm was found to be Langmuir isotherm, written in the linear form (10) [10,11,23]:

$$\frac{c_{inh}}{\theta} = \frac{1}{K_{ads}} + c_{inh} \quad (10)$$

From the linear dependence $c_{inh}/\theta = f(c_{inh})$ drawn using the experimental parameters computed from weight loss data and Tafel slopes (Fig. 6), the value of the adsorption constant was calculated. The regression coefficient R^2 for all methods was very close to 1, indicating that the adsorption process of L-histidine on metal surface obeys the Langmuir isotherm. The values of standard Gibbs free energy determined by the three methods are −28.7 kJ mol^{-1} by Tafel slopes, −28.5 kJ mol^{-1} by weight loss data and −30.8 kJ mol^{-1} by EIS measurements, revealing that the adsorption of inhibitor molecules on metal surface takes place due to electrostatic interactions between the amino acid molecules and electrode surface. Generally, values of the free energy less negative than −40 kJ mol^{-1} are associated with processes that occur by physical adsorption of the inhibitor on metal surface [36].

It is noted that the mechanism of corrosion inhibition of carbon steel in 0.5 M CH_3COOH/0.25 M CH_3COONa solution in the presence of L-histidine can be deduced on the basis of adsorption isotherms. It is well known that in an acid solution L-histidine exists as a protonated species like some other amino acids [17,20,21]. For acetic acid/sodium acetate the calculated value of pH is 4.46 and the protonation degree of the inhibitor is very close to 1, taking into account the following reaction equilibrium equations:

Table 4
Experimental values of EEC parameters for carbon steel in 0.5 M CH_3COOH/0.25 M CH_3COONa solution with/without various concentration of L-histidine.

Inh. conc. (M)	R_s (Ω)	T (F cm^{-2} s^{n-1})	n	R_p (Ω cm^2)	C_{dl} (μF cm^{-2})	η (%)
Blank	9.3 (1.5%)	1.16 × 10^{-4} (3.9%)	0.90 (0.7%)	264 (1.1%)	54.6	–
1 × 10^{-4}	12.5 (1.7%)	1.14 × 10^{-4} (4.0%)	0.85 (0.8%)	375 (1.3%)	35.7	29.6
1 × 10^{-3}	18.8 (1.0%)	1.64 × 10^{-4} (2.2%)	0.80 (0.5%)	642 (1.0%)	38.4	58.9
1 × 10^{-2}	4.5 (5.6%)	1.39 × 10^{-4} (2.5%)	0.85 (fixed)	828 (3.8%)	37.8	68.1

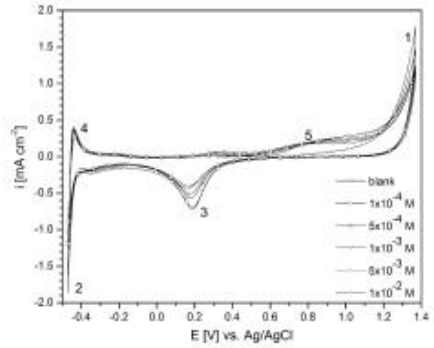

Fig. 4. Cyclic voltammograms on Pt electrode in 0.5 M CH_3COOH/0.25 M in the absence/presence of L-histidine, scan rate 50 mV s^{-1}.

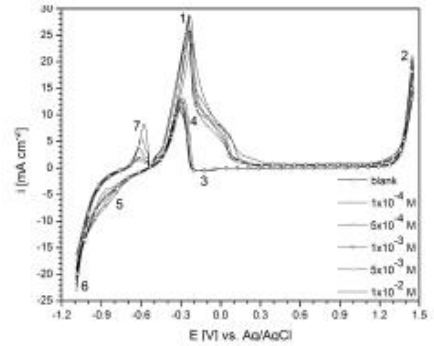

Fig. 5. Cyclic voltammograms on carbon steel electrode in 0.5 M CH_3COOH/0.25 M in the absence/presence of L-histidine, scan rate 50 mV s^{-1}.

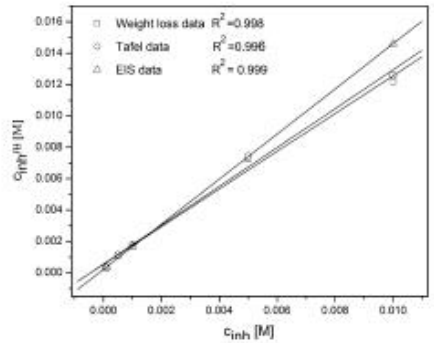

Fig. 6. Langmuir adsorption isotherm for L-histidine obtained by weight loss, EIS and Tafel data.

$H_3N{-}R(NH^+){-}COOH \overset{pK_{a2}}{\rightleftarrows} H_3N^+{-}R(NH$

$\overset{pK_{a1}}{\rightleftarrows} H_3N^+{-}R(N){-}COO^- \overset{pK_{a3}}{\rightleftarrows} H_2N{-}R($

The values of acidity constants are pK_{a3} = 9.08 [37]. As a consequence, in almost all amino acid molecul $(H_3N^+{-}R(NH^+){-}COO^-)$. Due to the elect carbon steel and inhibitor molecules, on the cathodic active sites of metal evolution reaction. At the same time molecules can adsorb on the steel surf nitrogen atoms of imidazole ring o unshared electron pairs.

3.6. Surface analysis

The surface morphology of the carb tigated after corrosive attack by the me time in the absence and presence of t graphs have been performed after th products formed on the sample surfa of L-histidine the surface of the sampl (Fig. 7a), while the presence of His fav compact layer that protects the sampl

(a)

(b)

Fig. 7. Microscope images after removing the (b) with 10^{-2} M L-histidine.

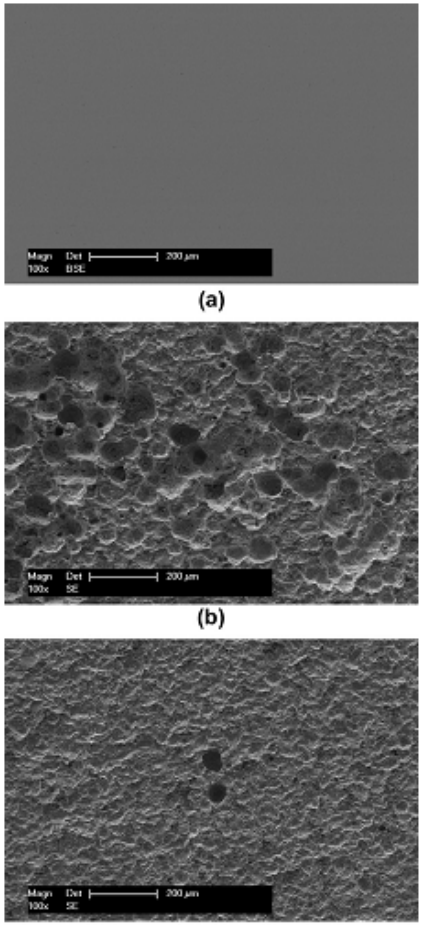

Fig. 8. SEM images obtained for carbon steel samples: abraded without immersion in test solutions (a); after 240 h immersion in the blank solution (b); and after 240 h immersion in the test solution with 10^{-2} M L-histidine (c).

Details about surface morphology were obtained by scanning electron microscopy.

Fig. 8 shows the SEM images recorded for the abraded surface of the carbon steel sample (a) and after removing the oxide layer from the surface. In the absence of inhibitor the image reveals clear pits and cavities with roughness due to metal dissolution under corrosive attack by the media (b). For 10^{-2} M concentration of inhibitor there are fewer corrosion marks observed on sample (c), suggesting that the carbon steel surface was protected by L-histidine molecules.

The atomic percentage of the elements is shown in Table 5.

Table 5
Atomic percentage of the elements.

	Fe	C	Cr	Si	Al	Mo	O
Blank	74.17	22.45	1.5	1.38	–	–	–
10^{-2} M inh.	45.77	38.94	1.6	4.85	1.35	1.56	5.93

4. Conclusions

L-histidine is a mixed safe corrosion inhibitor for carbon steel in weak acid solutions that acts both over the cathodic process of hydrogen evolution and the anodic process of metal dissolution. Inhibition efficiency was determined by three different methods: weight loss, linear polarization and electrochemical impedance, all giving comparable results. Inhibition efficiency increases with the amount of inhibitor and the maximum value was 81.6% for 10^{-2} M L-histidine. The amino acid adsorption on metal surface obeys Langmuir isotherm, and the value of Gibbs free energy reveal the electrostatic interactions between the charged molecules and the charged carbon steel. Generally, values of the free energy less negative than −40 kJ mol^{-1} are associated with processes that occur by physical adsorption of the inhibitor on metal surface. From surface analysis it results that amino acid suppresses the corrosion process by forming a protective film over the metal surface which prevents penetration of the corrosive media. The double layer capacitance obtained from EIS measurements decreases with the increasing of inhibitor concentration, arguing an adsorption process of the L-histidine on the metal surface.

The good inhibition efficiencies of L-histidine in acetic acid/sodium acetate solution makes it a suitable alternative as environmentally friendly corrosion inhibitor in deicing solutions in which sodium acetate is a main component. The advantages of this inhibitor consist in biodegradability and zero impact on the environment.

Acknowledgments

This work was partially supported by the strategic Grant POSDRU 107/1.5/S/77265 and POSDRU/21/1.5/G/13798, inside POSDRU Romania 2007–2013 co-financed by the European Social Fund – Investing in People.

References

[1] Y. Li, P. Zhao, Q. Liang, B. Hou, Berberine as a natural source inhibitor for mild steel in 1 M H_2SO_4, Appl. Surf. Sci. 252 (2005) 1245–1253.
[2] G. Moretti, F. Guidi, G. Grion, Tryptamine as a green iron corrosion inhibitor in 0.5 M deaerated sulphuric acid, Corros. Sci. 46 (2004) 387–403.
[3] M.A. Quraishi, A. Singh, V.K. Singh, D.K. Yadav, A.K. Singh, Green approach to corrosion inhibition of mild steel in hydrochloric acid and sulphuric acid solutions by the extract of *Murraya koenigii* leaves, Mater. Chem. Phys. 122 (2010) 114–122.
[4] A.K. Satapathy, G. Gunasekaran, S.C. Sahoo, K. Amit, P.V. Rodrigues, Corrosion inhibition by *Justicia gendarussa* plant extract in hydrochloric acid solution, Corros. Sci. 51 (2009) 2848–2856.
[5] L. Li, X. Zhang, J. Lei, J. He, S. Zhang, F. Pan, Adsorption and corrosion inhibition of *Osmanthus fragran* leaves extract, Corros. Sci. 63 (2012) 82–90.
[6] G. Quartarone, L. Ronchin, A. Vavasori, C. Tortato, L. Bonaldo, Inhibitive action of gramine towards corrosion of mild steel in deaerated 1.0 M hydrochloric acid solutions, Corros. Sci. 64 (2012) 82–89.
[7] J. Fu, S. Li, Y. Wang, L. Cao, L. Lu, Computational and electrochemical studies of some amino acid compounds as corrosion inhibitors for mild steel in hydrochloric acid solution, J. Mater. Sci. 45 (2010) 6255–6265.
[8] H. Ashassi-Sorkhabi, M.R. Majidi, K. Seyyedi, Investigation of inhibition effect of some amino acids against steel corrosion in HCl solution, Appl. Surf. Sci. 225 (2004) 176–185.
[9] O. Olivares-Xometl, N.V. Likhanova, M.A. Dominguez-Aguilar, E. Arce, Syntesis and corrosion inhibition of α-amino acids alkylamides for mild steel in acidic environment, Mater. Chem. Phys. 110 (2008) 344–351.
[10] M.S. Morad, Corrosion inhibition of mild steel in sulfamic acid solution by S-containing amino acids, J. Appl. Electrochem. 38 (2008) 1509–1518, http://dx.doi.org/10.1007/s10800-008-9595-2.

[11] M. ÖZcan, AC impedance measurements of cysteine adsorption at mild steel/sulphuric acid interface as corrosion inhibitor, J. Solid State Electrochem. 12 (2008) 1653–1661. doi: 10.1007/s10008-008-0551-1.
[12] M.S. Morad, Effect of amino acids containing sulfur on the corrosion of mild steel in phosphoric acid solutions containing Cl^-, F^- and Fe^{3+} ions: behaviour under polarization condition, J. Appl. Electrochem. 35 (2005) 889–895. doi: 10.1007/s10800-005-4745-2.
[13] O. Olivares, N.V. Likhanova, B. Gomez, J. Navarrete, M.E. Llanos-Serrano, E. Arce, J.M. Hallen, Electrochemical and XPS studies of decylamides of α-amino acids adsorption on carbon steel in acidic environment, Appl. Surf. Sci. 252 (2006) 2894–2909.
[14] J. Fu, S. Li, L. Cao, Y. Wang, L. Yan, L. Lu, L-Tryptophan as green corrosion inhibitor for low carbon steel in hydrochloric acid solution, J. Mater. Sci. 45 (2010) 979–986.
[15] R. Cui, N. Gu, C. Li, Polyaspartic acid as a green corrosion inhibitor for carbon steel, Mater. Corros. 61 (2010) 1–2. doi: 10.1002/maco.200905511.
[16] A.B. Silva, S.M.L. Agostinho, O.E. Barcia, G.G.O. Cordeiro, E. D'Elia, The effect of cysteine on the corrosion of 304L stainless steel in sulphuric acid, Corros. Sci. 48 (2006) 3668–3674.
[17] M.A. Amin, K.F. Khaled, Q. Mohsen, H.A. Arida, A study of the inhibition of iron corrosion in HCl solutions by some amino acids, Corros. Sci. 52 (2010) 1684–1695.
[18] G. Gece, S. Bilgic, A theoretical study on the inhibition efficiencies of some amino acids as corrosion inhibitors of nickel, Corros. Sci. 52 (2010) 3435–3443.
[19] G. Moretti, F. Guidi, Tryptophan as copper corrosion inhibitor in 0.5 M aerated sulfuric acid, Corros. Sci. 44 (2002) 1995–2011.
[20] K. Barouni, L. Bazzi, R. Salghi, M. Mihit, B. Hammouti, A. Albourine, S. El Issami, Some amino acids as corrosion inhibitors for copper in nitric acid solution, Mater. Lett. 62 (2008) 3325–3327.
[21] H. Ashassi-Sorkhabi, Z. Ghasemi, D. Seifzadeh, The inhibition effect of some amino acids towards the corrosion of aluminum in 1 M HCl + 1 M H_2SO_4 solution, Appl. Surf. Sci. 249 (2005) 408–418.
[22] Z. Ghasemi, A. Tizpar, The inhibition effect of some amino acids towards Pb–Sb–Se–As alloy corrosion in sulfuric acid solution, Appl. Surf. Sci. 252 (2006) 3667–3672.
[23] M.A. Kiani, M.F. Mousavi, S. Ghasemi, M. Shamsipur, S.H. Kazemi, Inhibitory effect of some amino acids on corrosion of Pb–Ca–Sn alloy in sulfuric acid solution, Corros. Sci. 50 (2008) 1035–1045.
[24] C.C. Ryerson, Ice protection of offshore platforms, Cold Reg. Sci. Technol. 65 (2011) 97–110.
[25] L. Fay, X. Shi, Environmental impacts of chemicals for snow and ice control: state of knowledge, Water Air Soil Poll. 222 (5) (2012). doi: 10.1007/s11270-011-1064-6.
[26] S.S. Bang, D. Johnston, Environmental effects of sodium acetate/formate deicer, Ice Shear, Arch. Environ. Contam. Toxicol. 35 (1998) 580–587.
[27] M.A. Quraishi, H.K. Sharma, Thiazoles as corrosion inhibitors for mild steel in formic and acetic acid solutions, J. Appl. Electrochem. 35 (2005) 33–39. doi: 10.1007/s10800-004-2055-8.
[28] M. Thirumalaikumar, S. Jeganmathan, Inhibition effect of nitrones on the corrosion of mild steel in organic acid media, Portugaliae Electrochem. Acta 29 (1) (2011) 1–8.
[29] R. Solmaz, E. Altunbaş, G. Kardaş, Adsorption and corrosion inhibition effect of 2-{[5-mercapto-1,3,4-thiadiazol-2-ylimino)methyl}phenol Schiff base on mild steel, Mater. Chem. Phys. 125 (2011) 796–801.
[30] M. Behpour, S.M. Ghoreishi, N. Soltani, M. Salavati-Niasari, M. Hamadanian, A. Gandomi, Electrochemical and theoretical investigation on the corrosion inhibition of mild steel by thiosalicylaldehyde derivatives in hydrochloric acid solution, Corros. Sci. 50 (2008) 2172–2181.
[31] S. Issaadi, T. Douadi, A. Zouaoui, S. Chafaa, M.A. Khan, G. Bouet, Novel thiophene symmetrical Schiff base compounds as corrosion inhibitor for mild steel in acidic media, Corros. Sci. 53 (2011) 1484–1488.
[32] G. Bereket, A. Yurt, The inhibition effect of some amino acids and hydroxyl carboxylic acids on pitting corrosion of aluminum alloy 7075, Corros. Sci. 43 (2001) 1179–1195.
[33] Y. Lang, D. Wang, Y. Wu, Q. Lai, L. Xue, S. Feng, Perylene-containing polysiloxane: an effective candidate for corrosion protection of iron surface, Appl. Surf. Sci. 257 (2011) 10576–10580.
[34] J. Ross MacDonald, Measuring techniques and data analysis, in: E. Barsoukov, J. Ross MacDonald (Eds.), Impedance Spectroscopy. Theory, Experiment and Applications, 2nd ed., John Wiley & Sons Inc., Hoboken, New Jersey, 2005, p. 198.
[35] A.Y. Musa, A.A.H. Kadhum, A.B. Mohamad, A.A.B. Rahoma, H. Mesmari, Electrochemical and quantum chemical calculations on 4,4-dimethyloxazolidine-2-thione as inhibitor for mild steel corrosion in hydrochloric acid, J. Mol. Struct.-Theochem. 969 (2010) 233–237.
[36] M.A. Amin, M.M. Ibrahim, Corrosion and corrosion control of mild steel in concentrated H_2SO_4 solutions by a newly synthesized glycine derivative, Corros. Sci. 53 (2011) 873–885.
[37] D. Harvey, Modern Analytical Chemistry, McGraw-Hill, 2000.

Universitatea Politehnica Timișoara

Piața Victoriei nr. 2
RO 300006 - Timișoara
Tel: +40 256 403000
Fax: +40 256 403021
rector@upt.ro
www.upt.ro

Universitatea Politehnica Timișoara

Succes la redactarea articolelor!

Circa 10.000 reviste WEB of SCIENCE (cu Factor de Impact) asteapta articolele dumneavoastra!

Bibliografie:

1. Alexandru Nichici, *Lucrări ştiinţifice – concepere, redactare, comunicare*, Editura Politehnica, 2010.
2. Steven Pinker, *Simţul stilului – Ghid de scriere pentru oamenii inteligenţi din secolul 21*, Editura Publica, 2015.

Pixuri pentru cei care termină şcoala online!


Va multumesc pentru atentie!